NAVAL POSTGRADUATE SCHOOL

MONTEREY, CALIFORNIA

THESIS

PROPAGATION ENVIRONMENT ASSESSMENT USING UAV ELECTROMAGNETIC SENSORS

by

Yi Kai Qiu

March 2018

Thesis Advisor:	David C. Jenn
Second Reader:	David A. Garren

Approved for public release. Distribution is unlimited.

THIS PAGE INTENTIONALLY LEFT BLANK

REPORT DOCUMENTATION PAGE			Form Approved OMB No. 0704–0188

Public reporting burden for this collection of information is estimated to average 1 hour per response, including the time for reviewing instruction, searching existing data sources, gathering and maintaining the data needed, and completing and reviewing the collection of information. Send comments regarding this burden estimate or any other aspect of this collection of information, including suggestions for reducing this burden, to Washington headquarters Services, Directorate for Information Operations and Reports, 1215 Jefferson Davis Highway, Suite 1204, Arlington, VA 22202-4302, and to the Office of Management and Budget, Paperwork Reduction Project (0704-0188) Washington, DC 20503.

1. AGENCY USE ONLY *(Leave blank)*	2. REPORT DATE March 2018	3. REPORT TYPE AND DATES COVERED Master's thesis

4. TITLE AND SUBTITLE PROPAGATION ENVIRONMENT ASSESSMENT USING UAV ELECTROMAGNETIC SENSORS	5. FUNDING NUMBERS
6. AUTHOR(S) Yi Kai Qiu	
7. PERFORMING ORGANIZATION NAME(S) AND ADDRESS(ES) Naval Postgraduate School Monterey, CA 93943-5000	8. PERFORMING ORGANIZATION REPORT NUMBER
9. SPONSORING /MONITORING AGENCY NAME(S) AND ADDRESS(ES) N/A	10. SPONSORING / MONITORING AGENCY REPORT NUMBER

11. SUPPLEMENTARY NOTES The views expressed in this thesis are those of the author and do not reflect the official policy or position of the Department of Defense or the U.S. Government. IRB number ____N/A____.

12a. DISTRIBUTION / AVAILABILITY STATEMENT Approved for public release. Distribution is unlimited.	12b. DISTRIBUTION CODE

13. ABSTRACT (maximum 200 words)

In this thesis, we attempt to build a picture of local propagation conditions by measuring signal transmission losses that allows naval operators to better understand the performance of their electromagnetic systems. By comparing the collected data against those of known baseline conditions, we can reliably determine the presence of atmospheric ducts as well as their ceiling heights, which include the detection of elevated ducts.

Another function of the post-processing analysis of the collected data is to estimate κ, which is a parameter of the atmospheric refractivity. Knowledge of κ allows us to estimate the radar horizon, which is the maximum distance that a transmitter and receiver can be separated and remain within the propagation line-of-sight, despite the curvature of the Earth. This important information allows operators to choose the optimal settings for the maximum detection range of their radar and radio systems.

We also investigate the measurement system requirements and operational scenarios such as the number of unmanned aerial vehicles and the total time needed to collect sufficient data. Two different types of flight patterns were studied, and our findings show that the vertical flight pattern using a rotary platform is more efficient. Furthermore, our simulation results suggest that the optimal operating frequency for the system is in the S Band.

14. SUBJECT TERMS propagation losses, atmospheric ducts, refractivity, radar horizon, UAV, effective Earth radius	15. NUMBER OF PAGES 83
	16. PRICE CODE

17. SECURITY CLASSIFICATION OF REPORT	18. SECURITY CLASSIFICATION OF THIS PAGE	19. SECURITY CLASSIFICATION OF ABSTRACT	20. LIMITATION OF ABSTRACT
Unclassified	Unclassified	Unclassified	UU

NSN 7540–01-280-5500 Standard Form 298 (Rev. 2–89) Prescribed by ANSI Std. 239–18

THIS PAGE INTENTIONALLY LEFT BLANK

Approved for public release. Distribution is unlimited.

PROPAGATION ENVIRONMENT ASSESSMENT USING UAV ELECTROMAGNETIC SENSORS

Yi Kai Qiu
Major, Republic of Singapore Air Force
B.Eng., National University of Singapore, 2006

Submitted in partial fulfillment of the
requirements for the degree of

MASTER OF SCIENCE IN ENGINEERING SCIENCE
(ELECTRICAL ENGINEERING)

from the

NAVAL POSTGRADUATE SCHOOL
March 2018

Approved by: David C. Jenn
Thesis Advisor

David A. Garren
Second Reader

R. Clark Robertson
Chair, Department of Electrical and Computer Engineering

THIS PAGE INTENTIONALLY LEFT BLANK

ABSTRACT

In this thesis, we attempt to build a picture of local propagation conditions by measuring signal transmission losses that allows naval operators to better understand the performance of their electromagnetic systems. By comparing the collected data against those of known baseline conditions, we can reliably determine the presence of atmospheric ducts as well as their ceiling heights, which include the detection of elevated ducts.

Another function of the post-processing analysis of the collected data is to estimate κ, which is a parameter of the atmospheric refractivity. Knowledge of κ allows us to estimate the radar horizon, which is the maximum distance that a transmitter and receiver can be separated and remain within the propagation line-of-sight, despite the curvature of the Earth. This important information allows operators to choose the optimal settings for the maximum detection range of their radar and radio systems.

We also investigate the measurement system requirements and operational scenarios such as the number of unmanned aerial vehicles and the total time needed to collect sufficient data. Two different types of flight patterns were studied, and our findings show that the vertical flight pattern using a rotary platform is more efficient. Furthermore, our simulation results suggest that the optimal operating frequency for the system is in the S Band.

THIS PAGE INTENTIONALLY LEFT BLANK

TABLE OF CONTENTS

I. INTRODUCTION....1
- A. MOTIVATION....1
- B. BACKGROUND AND PREVIOUS RESEARCH....2
- C. OBJECTIVE....4
- D. THESIS OUTLINE....4

II. BACKGROUND....5
- A. REFRACTION....5
- B. TYPES OF REFRACTIVE CONDITIONS....8
  - 1. Standard and Super-Refraction....9
  - 2. Sub-Refraction....9
  - 3. Trapping or Ducting....9
- C. ATMOSPHERIC DUCTS....9
  - 1. Surface Duct....11
  - 2. Elevated Duct....13
  - 3. Evaporation Duct....13
- D. CHAPTER SUMMARY....14

III. DATA COLLECTION AND PROCESSING....15
- A. BROAD CONCEPT FOR DATA COLLECTION....15
- B. FLOW DIAGRAM FOR DATA COLLECTION AND PROCESSING....16
- C. SIMULATED DATA COLLECTION USING AREPS....17
- D. DATA PROCESSING USING MATLAB....19
- E. CHAPTER SUMMARY....22

IV. SIMULATED TEST RESULTS....23
- A. METHOD TO DETERMINE THE EXISTENCE OF DUCTS....23
  - 1. Verifying Capability to Detect Surface Ducts....23
  - 2. Verifying Capability to Detect Elevated Ducts....24
  - 3. Minimum Data Points....27
- B. METHOD TO DETERMINE THE *K* VALUE....35
  - 1. Verifying the Capability to Estimate κ Value....36
  - 2. Minimum Data Points....38
- C. CHAPTER SUMMARY....41

V. SYSTEM IMPLEMENTATION REQUIREMENTS....43

A. SYSTEM DIAGRAM 43
B. FREQUENCY SELECTION 45
C. RECEIVER SENSITIVITY AND TRANSMITTER MINIMUM EFFECTIVE ISOTROPIC RADIATED POWER 50
D. SUPPORTING EQUIPMENT 51
1. GPS, Altimeter, and Gyroscope 51
2. Data Storage and Local Processing Capability 51
3. Data Link 52
4. Processing Computer 52
E. FLIGHT PATTERNS AND DATA COLLECTION TIME 52
1. Flight Pattern 52
2. Samples Required 55
3. Data Collection Time 55
F. CHAPTER SUMMARY 58

VI. CONCLUSIONS AND RECOMMENDATIONS 59
A. SUMMARY AND CONCLUSIONS 59
B. FUTURE WORK 60

LIST OF REFERENCES 61

INITIAL DISTRIBUTION LIST 63

LIST OF FIGURES

Figure 1. Influence of Propagation Conditions on Radar Detection. Source: [5]. 2

Figure 2. Propagation Losses under Standard Atmospheric Conditions 3

Figure 3. Propagation Losses when a Surface Duct Exists 4

Figure 4. Effects of Earth Curvature on Line of Sight. Adapted from [11]. 7

Figure 5. Refracted Ray Compensated by Effective Earth Radius. Adapted from [11]. 8

Figure 6. Electromagnetic Wave Paths under Different Refractive Conditions. Source: [12]. 8

Figure 7. Effect of Elevated Duct on Radar Coverage. Source: [13]. 10

Figure 8. Modified Refractivity Profile of Atmospheric Ducts. Adapted from [14]. (a) Standard atmosphere—no duct, (b) Evaporation duct, (c), (d) Surface ducts, (e) Elevated duct. The height of duct is indicated by the arrows on each profile. 11

Figure 9. Propagation Loss from an Emitter for Standard Conditions 12

Figure 10. (a) Propagation Loss from an Emitter in a Surface Duct, (b) Modified Refractivity Profile 12

Figure 11. Concept of Data Collection 15

Figure 12. Flow Diagram of Simulated and Actual Data Collection and Processing 16

Figure 13. Regions Using the Different Algorithms in APM. Source: [16]. 17

Figure 14. Graphical Display from AREPS of Propagation Losses from an Emitter 19

Figure 15. Graphical Display from MATLAB Code Comparing the Propagation Losses 20

Figure 16. Plot Showing Large Variations from Surface to 1000 ft, which Corresponds to Height of Surface Duct at a Fixed Distance of 300 nmi 21

Figure 17. Gradient of Propagation Losses Curves. Baseline 1.0, 4/3, 2.0 in Black and Processed Data in Red 22

Figure 18. Processed Results Showing a 500-ft Surface Duct. (a) Propagation Loss Difference and (b) Average Variation over Range at Each Height for a Range of 300 nmi. 24

Figure 19. Processed Results Showing a 1000-ft Surface Duct. (a) Propagation Loss Difference and (b) Average Variation over Range at Each Height for a Range of 300 nmi. 24

Figure 20. Processed Results Showing a 2000 ft Ceiling Elevated Duct. (a) Propagation Loss Difference and (b) Average Variation over Range at Each Height for a Range of 300 nmi. 26

Figure 21. Processed Results Showing a 3500 ft Ceiling Elevated Duct. (a) Propagation Loss Difference and (b) Average Variation over Range at Each Height for a Range of 300 nmi. 26

Figure 22. Processed Results Showing a 6100 ft Ceiling Elevated Duct. (a) Propagation Loss Difference and (b) Average Variation over Range at Each Height for a Range of 300 nmi. 27

Figure 23. Processed Results of Profile 1 of Table 3 with a 1000-ft Height Surface Duct. (a) Propagation Loss Difference and (b) Average Variation over Range at Each Height for a Range of 100 nmi. 28

Figure 24. Processed Results of Profile 2 of Table 3 with a 1000-ft Height Surface Duct. (a) Propagation Loss Difference and (b) Average Variation over Range at Each Height for a Range of 50 nmi. 29

Figure 25. Processed Results of Profile 3 of Table 3 with a 1000-ft Height Surface Duct. (a) Propagation Loss Difference and (b) Average Variation over Range at Each Height for a Range of 50 nmi.. 29

Figure 26. Processed Results of Profile 4 of Table 3 with a 1000-ft Height Surface Duct. (a) Propagation Loss Difference and (b) Average Variation over Range at Each Height for a Range of 40 nmi. 30

Figure 27. Propagation Loss Data from AREPS in 1000-ft Height Surface Duct 31

Figure 28. Processed Results of Profile 1 of Table 3 with a 2000-ft Ceiling Elevated Duct. (a) Propagation Loss Difference and (b) Average Variation over Range at Each Height for a Range of 100 nmi. 31

Figure 29. Processed Results of Profile 2 of Table 3 with a 2000-ft Ceiling Elevated Duct. (a) Propagation Loss Difference and (b) Average Variation over Range at Each Height for a Range of 50 nmi 32

Figure 30. Processed Results of Profile 3 of Table 3 with a 2000-ft Ceiling Elevated Duct. (a) Propagation Loss Difference and (b) Average Variation over Range at Each Height for a Range of 50 nmi. 32

Figure 31. Processed Results of Profile 4 of Table 3 with a 2000-ft Ceiling Elevated Duct. (a) Propagation Loss Difference and (b) Average Variation over Range at Each Height for a Range of 40 nmi. 33

Figure 32. (a) Propagation Loss in Standard Conditions, (b) Propagation Loss when 2000 ft Elevated Duct is Present, (c) Average Variations from Comparing both Data 34

Figure 33. Baseline Gradient Curves for $\kappa = 1.0$, $\kappa = 4/3$, and $\kappa = 2.0$ 36

Figure 34. Results of Gradient Curve for $\kappa = 1.0$ Based on AREPS $\kappa = 1$ Data 37

Figure 35. Results of Gradient Curves for $\kappa = 4/3$ Based on AREPS $\kappa = 4/3$ Data 37

Figure 36. Results of Gradient Curves for $\kappa = 2$ Based on AREPS $\kappa = 2$ Data 38

Figure 37. Unable to Fit Gradient Curves for (a) 50 nmi Range and (b) 100 nmi Range 39

Figure 38. Gradient Curve for 125 nmi Range 40

Figure 39. Envisaged System to Collect and Process Propagation Loss Data 44

Figure 40. Block Diagram of Equipment for Data Collection and Processing 44

Figure 41. Propagation Losses for (a) 450 MHz, (b) 1 GHz, (c) 5 GHz, and (d) 12 GHz 46

Figure 42. Processed Results to Identify 1000 ft Surface Duct with Frequencies (a) 450 MHz, (b) 1 GHz, (c) 3 GHz, (d) 5 GHz, (e) 7 GHz, and (f) 12 GHz..... 48

Figure 43. Processed Results to Identify 2000 ft Ceiling Elevated Duct with Frequencies (a) 450 MHz, (b) 1 GHz, (c) 3 GHz, (d) 5 GHz, (e) 7 GHz, and (f) 12 GHz 49

Figure 44. Data Collection in an Azimuth Measurement Plane 53

Figure 45. Horizontal Flight Pattern 54

Figure 46. Vertical Flight Pattern 54

Figure 47. Horizontal Flight Pattern with Estimated Time (Single ScanEagle) 56

Figure 48. Vertical Flight Pattern with Estimated Time (Single Quadrotor) 57

Figure 49. Vertical Flight Pattern with Estimated Time (Multiple Quadrotors) 57

THIS PAGE INTENTIONALLY LEFT BLANK

LIST OF TABLES

Table 1. System Parameters Used in AREPS for Data Collection 13
Table 2. Ceiling and Floor Altitudes of Elevated Duct Profiles 25
Table 3. Selected Profiles of Interest 28
Table 4. Minimum Data Points for the Cases Investigated.....35
Table 5. Default Simulation Setup.....39
Table 6. Minimum Samples Requirement for Both Functions 40
Table 7. Key Functions of Envisaged System 45
Table 8. Parameters Used for Data Collection.....47
Table 9. EIRP Required for Various Types of Spectrum Analyzers 50
Table 10. Distance Traveled by ScanEagle, One Measurement 54
Table 11. Data Collection Times for Horizontal Flight Pattern.....56
Table 12. Data Collection Time for Vertical Flight Pattern 57

THIS PAGE INTENTIONALLY LEFT BLANK

LIST OF ACRONYMS AND ABBREVIATIONS

APM	Advanced propagation model
AREPS	Advanced refractive-effects prediction system
dB	Decibels
dBm	Decibel-milliwatts
EIRP	Effective isotropic radiated power
EM	Electromagnetic
FE	Flat earth
Ft	Feet
GPS	Global positioning system
HF	High frequency
IREPS	Integrated refractive-effects prediction system
km	Kilometer
LOS	Line-of-sight
MDS	Minimum discernible signal
nmi	Nautical mile
PE	Parabolic equation
RO	Ray optics
SNR	Signal-to-noise ratio
SPAWAR	Space and Naval Warfare Systems Center
SSD	Solid state drive
UAV	Unmanned air vehicle
UHF	Ultra high frequency
VHF	Very high frequency
XO	Extended optics

THIS PAGE INTENTIONALLY LEFT BLANK

ACKNOWLEDGMENTS

I would like to express my most sincere gratitude to my thesis advisor, Professor David C. Jenn for his patience and guidance over the past year. I truly admire his immense knowledge in this field and his guidance helped me tremendously in my research and writing of this thesis. I really appreciate his efforts, despite his busy schedule, to go through this thesis with me in great detail to ensure quality. I could not have imagined a better advisor and mentor. I would also like to thank my second reader, Professor David A. Garren, for taking precious time from his busy schedule to read this thesis and provide me with his valuable advice and input.

Last but not least, I would like to express my deepest appreciation to my lovely wife, Anna Fong, for her wholehearted support and being so understanding during the course of my studies here in Naval Postgraduate School. This journey would not have been possible without her.

THIS PAGE INTENTIONALLY LEFT BLANK

I. INTRODUCTION

A. MOTIVATION

Understanding propagation conditions, or refractivity, in the atmospheric surface layer is important for the prediction of the performance of sensors such as radar and communications systems. The existence of the atmospheric layer causes electromagnetic signals to bend and, as a result, degrades the performance of these sensors; therefore, it is imperative for the operators to know the existing atmospheric propagation conditions and understand the impact of such conditions on their radar and communications systems. The effects include reduced range, limited field of view, and degraded accuracy and resolution. Operators can then apply mitigation measures to reduce the impact on current operations.

There have been many studies on this topic due to its importance to naval operations. The studies were mostly theoretical without consideration of measurement [1], [2], [3]. In our research, we found very few existing studies or research that looked into the use of unmanned aerial vehicles (UAV) to sense the state of the electromagnetic (EM) atmosphere. Perhaps this is due to the high cost of outfitting UAVs with a suite of sensors. One such study involved outfitting UAVs with radiosondes to measure the prevailing meteorological conditions; the data from this study were used to estimate the atmospheric refractivity [4].

With the proliferation of UAVs in recent years, their use has become more affordable. It is now feasible to look into the possibility of using UAVs to predict the prevailing atmospheric conditions due to their ability to cover large areas within a short span of time, providing near real-time information on atmospheric propagation conditions. Electromagnetic (EM) conditions can affect the performance of radar and communications systems as illustrated in Figure 1. In the figure, we observe that the radar detection area is different depending on the refractivity index versus height, and this is caused by the atmospheric meteorological conditions. Targets may be missed in extreme refractivity conditions; therefore, it is important to know the current (real-time)

propagation environment to minimize any operational impact to radars and communications systems.

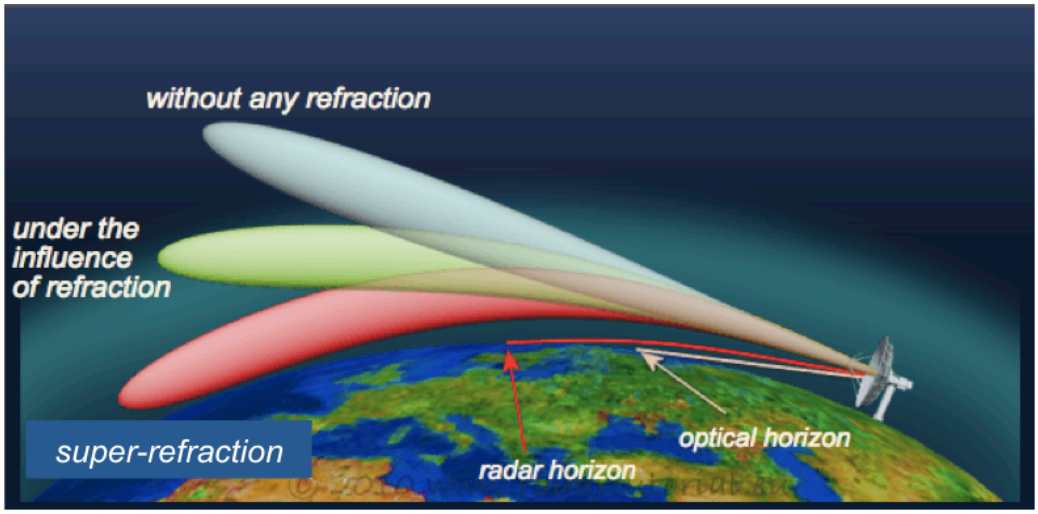

Figure 1. Influence of Propagation Conditions on Radar Detection. Source: [5].

B. BACKGROUND AND PREVIOUS RESEARCH

Due to the significant impact of atmospheric refractivity on naval and maritime operations, there have been many studies to better estimate and predict this factor. One of the most common methods in the field of meteorology is to collect environmental data such as air and sea temperature, wind speed, and humidity with reference to height by radiosonde. This data is used to estimate the atmospheric refractivity. The estimation model using meteorological parameters is very sensitive as any slight differences in the parameters can lead to large errors and, therefore, may not be the best approach to determine atmospheric refractivity [6].

Another common method is the use of radar returns to infer the atmospheric refractivity [7]. This is commonly known as refractivity-from-clutter (RFC), where previously saved profiles are matched with reflected clutter signals from radar. These clutter signals vary with atmospheric refractivity, and the RFC technique attempts to match the return clutter power with large databases to determine the atmospheric refractivity that causes the return clutter. Other less common methods include the use of

ultra-high frequency (UHF) signal strength and global positioning system (GPS) signals to estimate the atmospheric refractivity [8].

In this thesis, we explore the technique of using measured electromagnetic propagation losses to estimate the atmospheric refractivity. According to Lee Ted Rogers, a senior scientist from the Space and Naval Warfare Systems Center, this technique has the "potential to be more representative of range- and time-varying refractive environments than estimates obtained using in-situ sensing" [9]. In-situ sensing is typically referred to as on-site sensing. The estimation model using local parameters is not reliable for predicting long distance propagation effects under most circumstances.

To overcome the shortcomings of in-situ sensing, sensors could be fitted onboard UAVs to measure real-time EM propagation losses over large regions. This information could then be used to extract the real-time atmospheric refractivity profile as it is directly related to the characteristics of propagation losses. This concept is illustrated in Figure 2 and Figure 3, where propagation losses (in dB) at various ranges and heights are shown graphically in the plots. The propagation losses for standard atmospheric conditions is shown in Figure 2, and propagation losses when a surface duct exists is shown in Figure 3. A comparison of the propagation losses in the figures clearly illustrates the effect of atmospheric refractivity conditions on propagation.

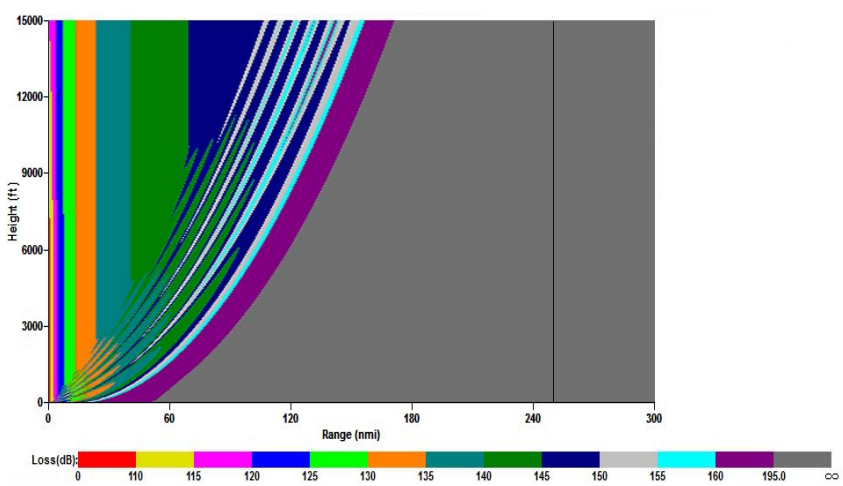

Figure 2. Propagation Losses under Standard Atmospheric Conditions

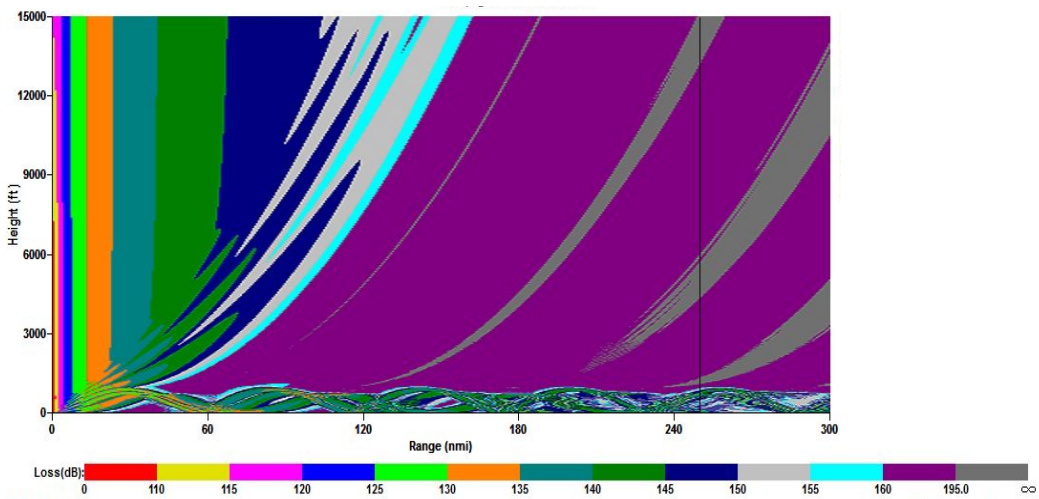

Figure 3. Propagation Losses when a Surface Duct Exists

C. OBJECTIVE

In this thesis, we propose to utilize UAVs to measure signal transmission losses between transmitters and a number of receivers at various ranges and heights. Through data processing, the current (real-time) atmospheric conditions such as ducts and refractive index can then be extracted. We also examine the basic architecture of the envisaged system for data collection and processing and the minimum data required as well as the best approach to collect these data.

D. THESIS OUTLINE

In Chapter II, we explain the reasons and theories on how atmospheric conditions and refractivity cause electromagnetic signals to bend and propagate over the horizon. In Chapter III, we present the simulation methodology, which includes how the data are simulated and processed to extract refractivity. In Chapter IV, the simulated experimental data from the Advanced Refractive Effects Prediction System (AREPS) software are presented and analyzed to show that the refractivity profile and atmospheric ducts can be obtained by processing the data. There is also a study on the system implementation and measurement requirements in Chapter V. The conclusions and recommendations for future work are provided in Chapter VI.

II. BACKGROUND

The background and theory of electromagnetic propagation in the troposphere (i.e., the approximately 10 km nearest to the Earth's surface) and how electromagnetic waves are affected by the presence of atmospheric refractive layers and ducting are provided in this chapter.

A. REFRACTION

Refraction refers to the bending of electromagnetic waves when they pass through different transmission media. The index of refraction n determines how the properties of electromagnetic waves bend in a medium and is defined as [10]

$$n = \frac{c}{v}, \tag{1}$$

where c refers to the speed of propagation in free space and v is the speed of propagation (phase velocity) in the medium.

The refractive index near the Earth's surface is typically around 1.000350, and as height increases, it approaches unity. Due to the small changes that occur, it is, therefore, more practical to use the parameter called refractivity (in N-units), which is defined as

$$N = (n-1) \times 10^6. \tag{2}$$

The refractive index in terms of "N-units" is also related to the atmospheric meteorological conditions as [9]

$$N = 77.6\left(\frac{P}{T} + \frac{4810e}{T^2}\right), \tag{3}$$

where P is the atmospheric pressure in hectopascals, e is the partial water vapor pressure in hectopascals, and T is the temperature in K.

In the field of propagation assessment, it is also useful to use the modified refractivity M which is related to N and height above the surface. The modified refractivity (in M-units) is defined as [9]

$$M = N + 0.157h \,, \tag{4}$$

where h is the height above the surface in m.

To determine the refractivity and how electromagnetic waves bend over the spherical Earth versus height from the surface, we can also use the κ factor, given by [10]

$$\kappa = \frac{1}{1 + \left(\frac{R_e}{n}\right)\left(\frac{dn}{dh}\right)}, \tag{5}$$

where R_e is the radius of the Earth, which is approximately 6,370 km. For standard atmospheric conditions, dN/dh is approximately −39 N units/km. Using Eq. (2), we get the [10]:

$$\frac{dN}{dh} = \frac{dn}{dh} \times 10^6. \tag{6}$$

The values of dN/dh can vary depending on atmospheric conditions, and this causes corresponding κ values to vary accordingly [10]. Knowing the κ value of the atmosphere allows us to understand how the electromagnetic waves propagate and, hence the performance of radar and communications systems under different atmospheric conditions. A κ value of 4/3 is representative of the refractivity gradient under standard atmospheric conditions.

The κ value is also significant in determining the radar, or radio horizon, which is the maximum distance that a transmitter and receiver can be separated and remain within the propagation line-of-sight despite the curvature of the Earth. From Figure 4, we observe that the geometric line-of-sight from the transmitter to the receiver is blocked by the Earth's curvature. In reality, the electromagnetic waves are refracted due to the atmosphere. To use straight lines when tracing wave paths, we compensate for the

refraction by adjusting the Earth radius, which is known as the effective Earth radius R_e' where [11]

$$R_e' = \kappa R_e. \tag{7}$$

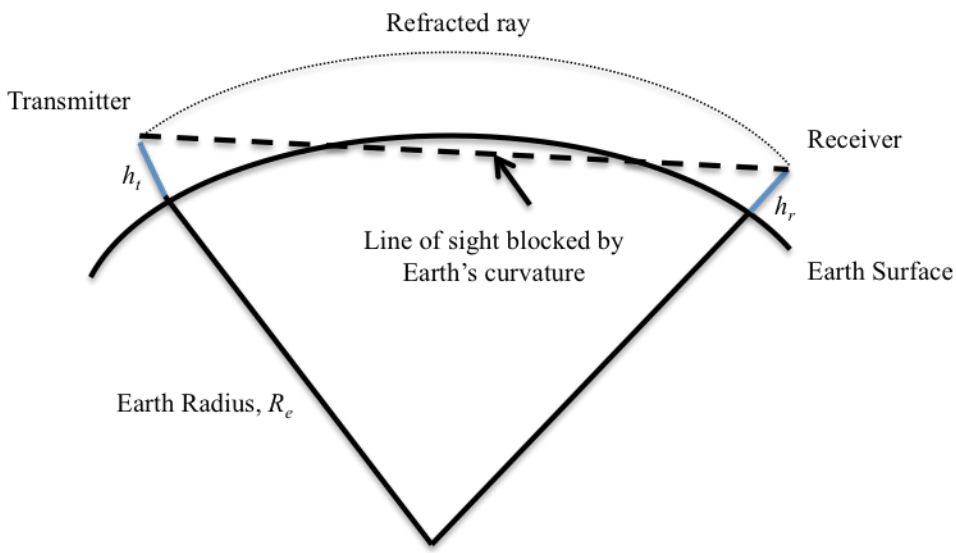

Figure 4. Effects of Earth Curvature on Line of Sight. Adapted from [11].

In Figure 5, the effective Earth radius compensates for the atmospheric conditions, and the refracted ray is effectively a straight line. The idea of the effective Earth radius is important as this allows us to calculate the radar horizon, which is defined as [11]

$$R_{RH} \approx \sqrt{2R_e'h_t} + \sqrt{2R_e'h_r} \ , \tag{8}$$

where h_t is the height of the transmitting antenna and h_r is the height of the receiving antenna.

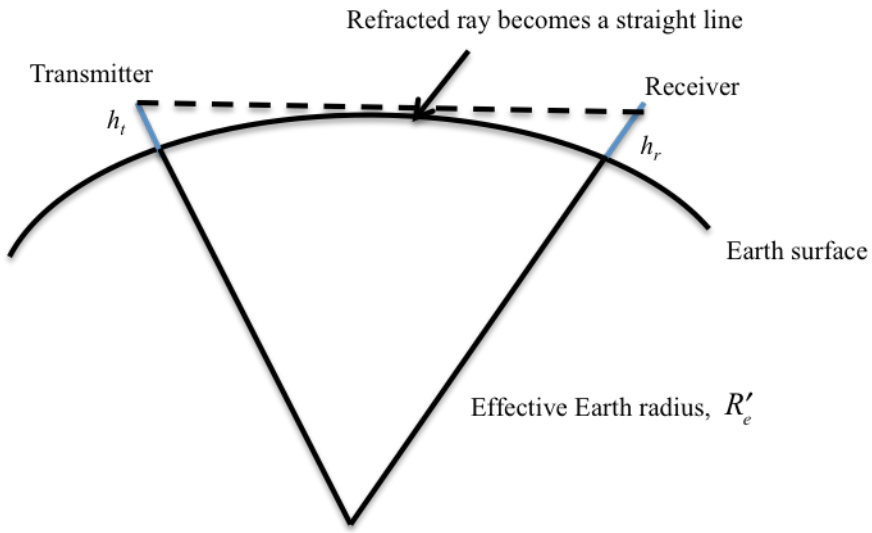

Figure 5. Refracted Ray Compensated by Effective Earth Radius. Adapted from [11].

B. TYPES OF REFRACTIVE CONDITIONS

There are four types of refractive conditions: (1) standard or normal, (2) super-refraction, (3) sub-refraction, and (4) trapping/ducting (anomalous) [10]. These conditions affect how the electromagnetic waves bend and are related to how the index of refraction varies with height. The effects of these conditions on the bending of electromagnetic wave paths are illustrated in Figure 6.

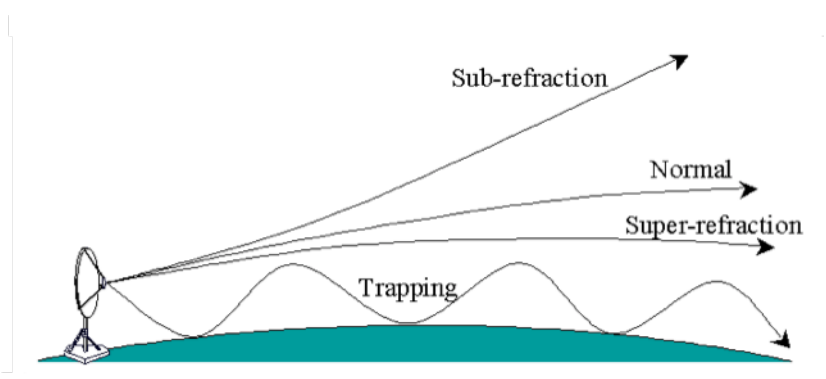

Figure 6. Electromagnetic Wave Paths under Different Refractive Conditions. Source: [12].

1. Standard and Super-Refraction

When standard and super-refraction occur, the electromagnetic waves bend downward towards the Earth's surface [10]. In the case of super-refraction, the wave bends more as compared to the standard condition. The phenomenon of electromagnetic waves bending towards the Earth happens when the N-gradient is between 0 and −157 N/km or the M-gradient is between 0 to 118 M/km. The corresponding κ values are 1 to ∞. The larger the value of κ, the more the electromagnetic waves bend towards the surface. Typically, the electromagnetic waves are considered to have undergone super-refraction when κ is greater than 2.0 or N is between −79 to −157 N/km [10].

2. Sub-Refraction

When sub-refraction occurs, the electromagnetic waves bend away from the Earth's surface [10]. This phenomenon happens when the N-gradient is greater than 0 N/km or the M-gradient is greater than 157 M/km. The corresponding κ value is between 0 and 1. The smaller κ is, the more the waves bend upwards away from the Earth's surface. When κ is exactly 1, the profile is such that the effective Earth radius is equal to the actual radius of the Earth [10].

3. Trapping or Ducting

In trapping or ducting conditions, the electromagnetic waves are confined to a narrow region of the troposphere and bend back and forth between the upper and lower layer [10]. This is due to electromagnetic waves being bent towards the Earth's surface much more rapidly than the curvature of the Earth. This happens when the N-gradient is less than −157 N/km, the M-gradient is less than 0 M/km, or the value of κ is between $-\infty$ to 0. During such conditions, the electromagnetic waves confined within this region can travel much farther than the waves outside a duct due to the absence of isotropic spreading [10].

C. ATMOSPHERIC DUCTS

The presence of atmospheric ducts indicates trapping conditions where electromagnetic waves are "trapped" in a confined region and propagate to a much

farther distance than in normal conditions. This might seem like a positive condition for radars because it allows a longer-range detection. Yet, as seen in Figure 7, the trapped waves can lead to coverage holes outside the duct. In this scenario, normal radar coverage under standard atmospheric conditions allows the ship to detect all three missiles (normal coverage in lighter green). By contrast, under the condition of the elevated duct, radar coverage is affected and can only detect missile number 2 (in darker green). It is, therefore, important to understand the effects of atmospheric ducts on radar coverage which may otherwise cause targets to be missed, with a dire operational impact.

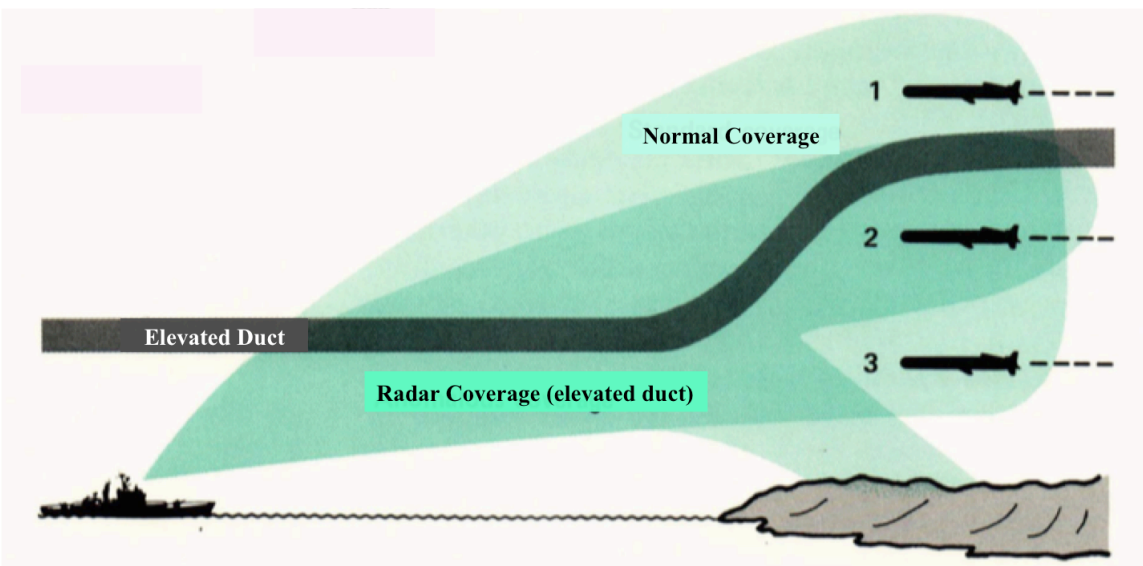

Figure 7. Effect of Elevated Duct on Radar Coverage. Source: [13].

As discussed previously, atmospheric ducts occur when the N-gradient is less than −157 N/km, the M-gradient is less than 0 M/km, or the value of κ is $-\infty$ to 0. The ducts are due to meteorological conditions such as atmospheric pressure, humidity, and temperature. The specific meteorological conditions determine the type of duct: (1) surface, (2) evaporation, or (3) elevated [7].

A common way to predict the type of atmospheric ducts is to plot the modified refractivity M against the height where the ducts occur. The range of heights where the

M-gradient is negative is where the atmospheric ducts occur; thus, the height where the ducts occur determines the type of ducts as seen in Figure 8.

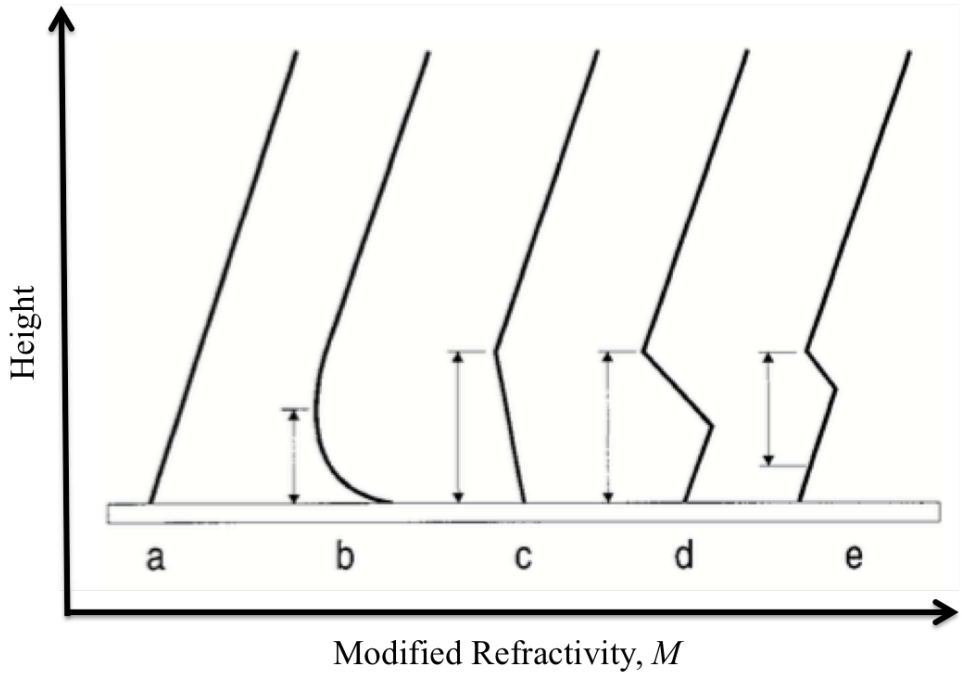

Figure 8. Modified Refractivity Profile of Atmospheric Ducts. Adapted from [14]. (a) Standard atmosphere—no duct, (b) Evaporation duct, (c), (d) Surface ducts, (e) Elevated duct. The height of duct is indicated by the arrows on each profile.

1. Surface Duct

Surface ducts extend down from a height to the Earth's surface and are common in the coastal areas due to sharp differences in temperature and humidity gradients between the warmer and dryer upper air layer and the sea. Surface ducts occur when temperature increases and humidity decreases rapidly with height [10]. This results in a trapping condition where the electromagnetic waves are trapped in the surface duct, which leads to the waves bending back and forth between the upper and lower layer. An example of propagation losses of electromagnetic waves from an emitter under standard atmospheric condition is shown in Figure 9, and propagation losses from an emitter in a surface duct is shown in Figure 10. The system parameters for this example are shown in

Table 1. . From the figures, we observe that the wave paths are longer within the surface duct as compared to standard conditions. In standard conditions, and under the conditions in Table 1, the radar is not expected to be able to detect target 100 nmi from the emitter; however, when the surface duct is present, this radar can detect a target that is flying at 500 ft and 100 nmi away.

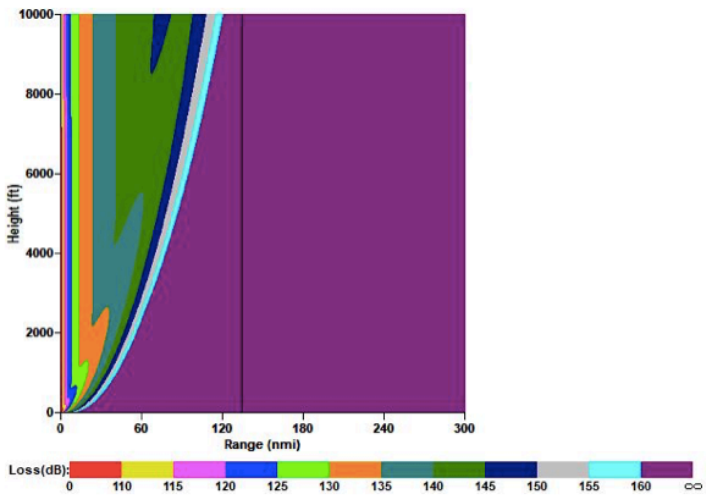

Figure 9. Propagation Loss from an Emitter for Standard Conditions

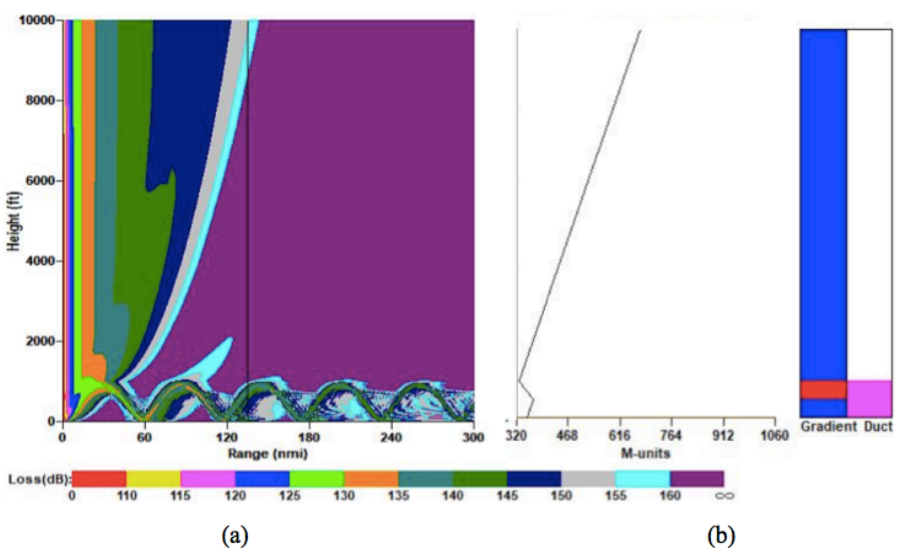

Figure 10. (a) Propagation Loss from an Emitter in a Surface Duct, (b) Modified Refractivity Profile

Table 1. System Parameters Used in AREPS for Data Collection

	Symbol	Type / Parameters
System Type	-	Radar
Frequency	f	3 GHz
Peak Power	P_t	2000 kW
Pulse Length	τ	9 μs
Receiver Noise Figure	NF	5.5 dB
Assumed System Loss	L	3 dB
Maximum Antenna Gain	G	39 dB
Horizontal Beam Width	ϕ_B	2°
Vertical Beam Width	θ_B	1.5°
Antenna Elevation Angle	θ_o	0.5°
Antenna Polarization	H	Horizontal
Antenna Height	h_a	10 ft
Range Output Points	N_r	440
Height Output Points	N_h	384

2. Elevated Duct

Similar to surface ducts, elevated ducts are also due to a sharp difference in temperature and humidity gradients between upper and lower layers, except that the ducts exist at a high elevation such that electromagnetic waves from the surface cannot be trapped [10]. If the elevated duct is sufficiently low in altitude, it could potentially prevent radar from detecting air targets as shown in Figure 7.

3. Evaporation Duct

Evaporation ducts form when the humidity of the air decreases rapidly just above the surface of the sea. The heights of the evaporation ducts typically vary between 0 to 40 m, which is usually much smaller than surface ducts. Evaporation ducts have minimal impact on electromagnetic waves with frequencies below 2 GHz, but their effect increases with higher frequencies [7].

D. CHAPTER SUMMARY

In this chapter, the basic properties of the atmosphere were introduced and the effects of the different atmospheric conditions on wave propagation were also discussed. In the next chapter, the data collection and processing required to extract real-time atmospheric data are presented.

III. DATA COLLECTION AND PROCESSING

The data for this thesis were collected from simulation results from the Advanced Refractive Effects Prediction System (AREPS), which was developed by the Space and Naval Warfare Systems Center, San Diego (SPAWAR). In the course of this thesis, we conducted simulations under different conditions, and the data collected were processed using previously developed MATLAB codes with some minor improvements from the author of this thesis.

A. BROAD CONCEPT FOR DATA COLLECTION

The broad concept for data collection to extract the real-time atmospheric propagation conditions is illustrated in Figure 11. Transmitters and receivers are distributed throughout the environment of interest. The receivers and transmitters can be on UAVs, manned aircraft, the ships, or even shore-based transmitters of opportunity. The purpose of the transmitters and receivers is to determine propagation loss in the environment of interest, which we can then use to infer the atmospheric propagation conditions by processing the path loss data using the MATLAB program.

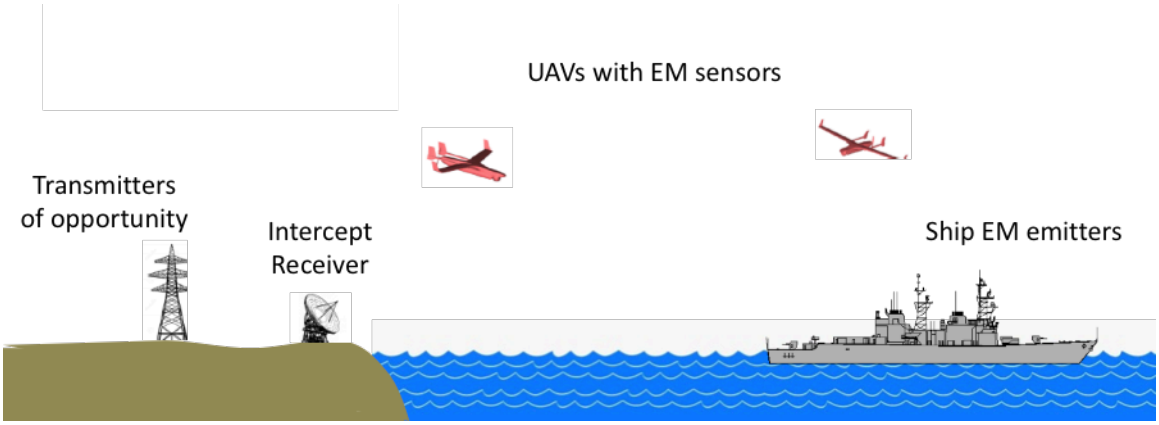

Figure 11. Concept of Data Collection

B. FLOW DIAGRAM FOR DATA COLLECTION AND PROCESSING

In this thesis, the data collection process under different atmospheric conditions is simulated by AREPS, and the output data are processed using the MATLAB program. The goal is to determine (1) the existence of an atmospheric duct, if any, and (2) the κ value. This process is illustrated in Figure 12 in the blue boxes on the left.

The red boxes on the right of Figure 12 illustrate the equivalent processes under real-life scenarios in which the UAVs collect propagation loss data. First, the measurement procedures such as area of operations and flying profiles have to be planned. The UAVs then fly to the environment of interest and execute the flying profiles to collect propagation loss data with respect to distances and heights from the emitter and send these data to a central processing computer. The central processor combines the data from multiple transmitter-receiver pairs to form a matrix of data in range and height. (Although an azimuth variation could be added, we limit this study to two dimensions.) The computer program then processes the data and determines the existence of any atmospheric ducts and the corresponding κ value.

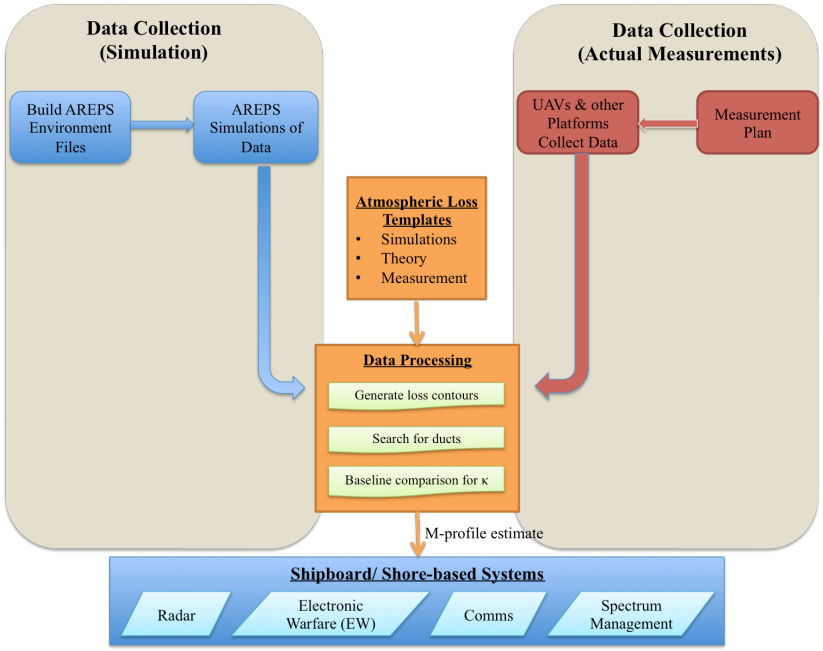

Figure 12. Flow Diagram of Simulated and Actual Data Collection and Processing

C. SIMULATED DATA COLLECTION USING AREPS

SPAWAR Systems Center, San Diego, introduced the Integrated Refractive Effects Prediction System (IREPS) in 1987, which provided the U.S. Navy with the capability to assess the effects of the different atmospheric conditions on shipboard electromagnetic equipment [15]. AREPS is the newer and improved version, which subsequently replaced the IREPS.

AREPS uses the Advanced Propagation Model (APM), a composite model using ray optics (RO), flat earth (FE), extended optics (XO), and the split step Fourier parabolic equation algorithm to solve, compute, and display propagation losses in a given atmospheric environment [16]. The program also has the capability to provide other results, such as radar probability of detection for radar and signal-to-noise ratio (SNR) for communications and electronic warfare systems.

The APM uses the Fourier parabolic equation (PE) algorithm to determine the propagation losses under the maximum propagation angle with corresponding maximum heights and ranges. The remaining regions (FE, RO, and XO) can then be pre-defined and calculated using the respective algorithms, as illustrated in Figure 13.

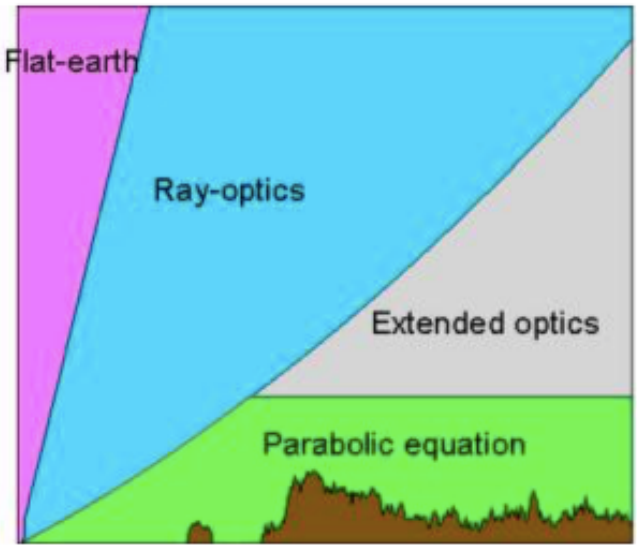

Figure 13. Regions Using the Different Algorithms in APM. Source: [16].

AREPS allows the user to create any kind of environmental condition by entering meteorological data such as air and sea temperatures, wind speed, and humidity with reference to height. AREPS then calculates and determines the refractivity profile. Alternatively, the user can also enter the *M* units with reference to height, which is the modified *M* refractivity profile as seen in Figure 8. The refractivity profiles affect how the electromagnetic waves bend and determine whether there are any atmospheric ducts present.

Using the desired refractivity profile, we can then create the parameters according to the experimental requirements and run the simulation to obtain the "synthetic" measured data. The output parameters adjusted for the simulations are as follows:

1. APM output specifications. These determine the number of range and height output points. In real data collection, this is the total number of data samples collected in range N_r and height N_h. During the course of the simulations, this was adjusted to determine the minimum number of samples, spacing of samples, and the most efficient data collection method.

2. Graphic display. This determines the maximum height and range of data collected (i.e., vertical and horizontal). This output parameter was adjusted to determine the most efficient method of data collection (i.e., the minimum data required to accurately determine the refractivity profile).

The results from a simulation include a graphical display of the propagation losses (in dB) with reference to range and height from the emitter. A sample of this display is shown in Figure 14 for the *M*-profile in Figure 10b and system parameters in Table 1.

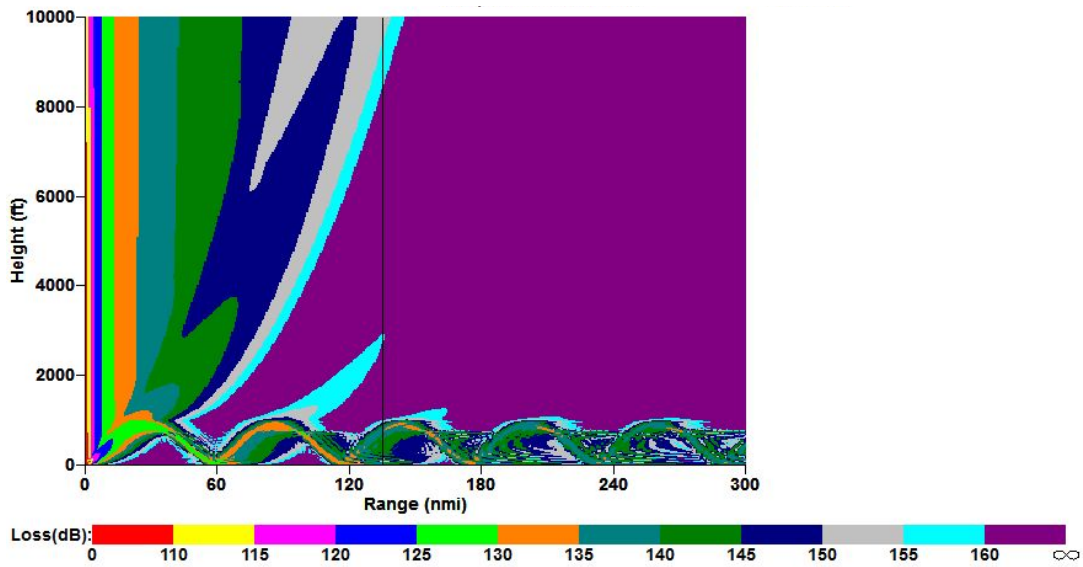

Figure 14. Graphical Display from AREPS of Propagation Losses from an Emitter

AREPS also saves a copy of the simulation data in a folder on the hard drive. These data are subsequently treated as data collected by a signal power detector or spectrum analyzer on the receiver mounted on a UAV. The signal source could be located on a ship, another UAV, a manned aircraft, or even a buoy. The measured data are processed by a computer program, which is discussed in the next section. The program is able to determine the propagation loss between the various emitters and receivers. Finally, interpolation, extrapolation, and other curve fitting tools are applied to get the loss pattern that can be compared to the baseline data (i.e., "loss templates").

D. DATA PROCESSING USING MATLAB

With knowledge of the data of the propagation loss with respect to range and height from the emitter, we now aim to solve for the inverse problem and determine the atmospheric refractivity. The MATLAB codes read the AREPS data and perform two key functions.

The first is to determine the existence of ducts by calculating and comparing the differences of the propagation loss data of an unknown refractivity profile scenario against propagation losses for known conditions. A sample AREPS processed data from

the MATLAB code from a surface duct scenario with a duct height of 1000 ft is given in Figure 15 and Figure 16. The contours in Figure 15 show the difference in propagation loss as compared to standard conditions. The contours seen in the figure predict an expected bending of electromagnetic waves in the surface duct.

We can clearly see that the top of the surface duct is about 1000 ft, which corresponds to the actual conditions in AREPS. The plots in Figure 16 show the average variations or differences of the propagation losses of the simulated data relative to standard conditions at each height for a fixed distance of 300 nmi. We can also clearly see that a surface duct exists with a height of 1000 ft. This is because the largest deviation from standard conditions occurs inside the duct.

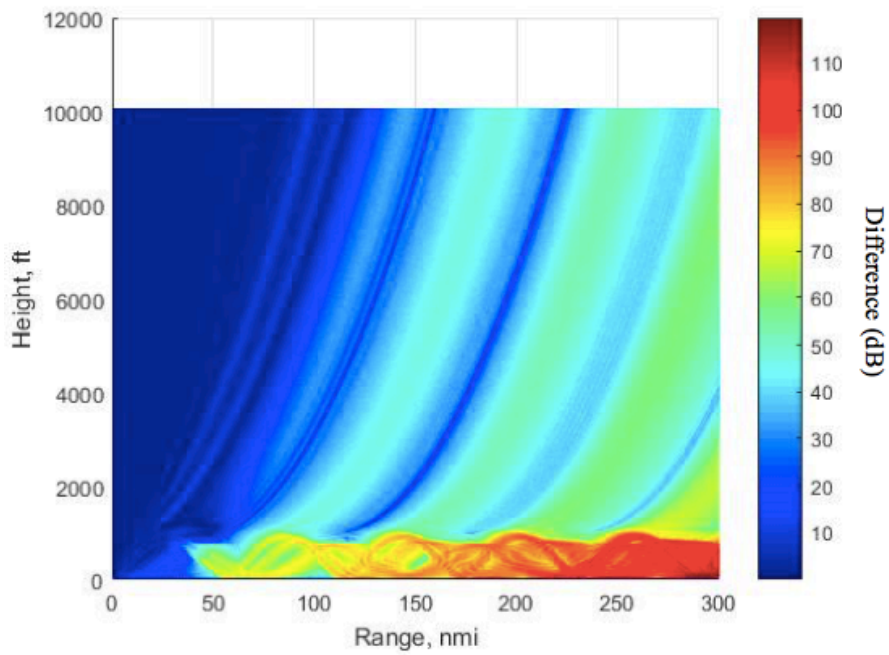

Figure 15. Graphical Display from MATLAB Code Comparing the Propagation Losses

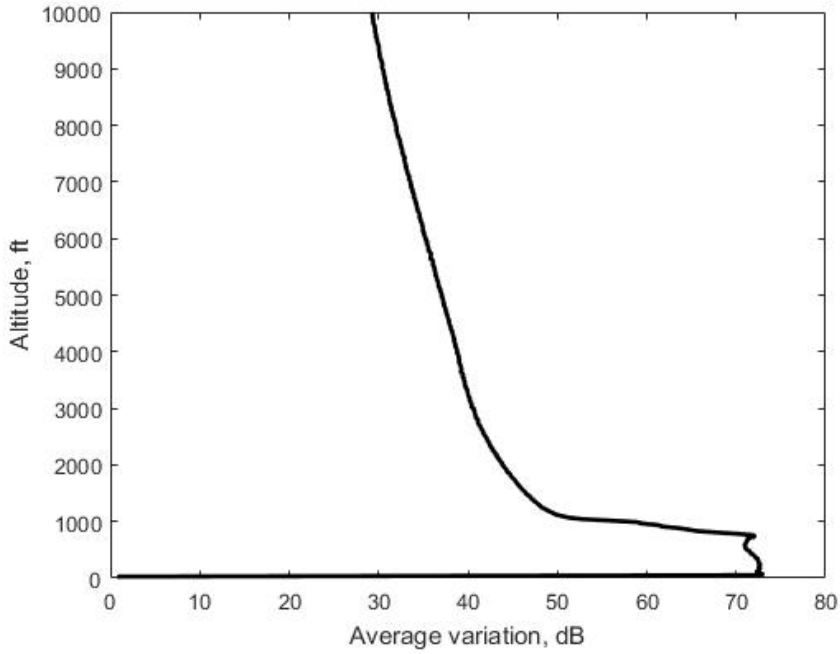

Figure 16. Plot Showing Large Variations from Surface to 1000 ft, which Corresponds to Height of Surface Duct at a Fixed Distance of 300 nmi

The second function of the MATLAB code is to determine the factor κ, which affects how the electromagnetic waves bend in the atmosphere. This is done by comparing the gradients of the propagation loss curves against known baseline propagation loss curves of factor of κ, for example 1.0, 4/3, and 2.0. The gradient curves are obtained by calculating the range closest to the average signal strength at each height. The resulting data are then fitted into a curve using the MATLAB "polyfit" function. A sample result is shown in Figure 17, where we can see that the gradient of the propagation losses from the collected AREPS data fits the curve of κ = 4/3, and this corresponds correctly with the environment refractivity profile on which these data are based. This example is optimistic because no measurement errors exist and the data-sampling interval is small. There is also no interpolation between data points required, which would otherwise add to the errors.

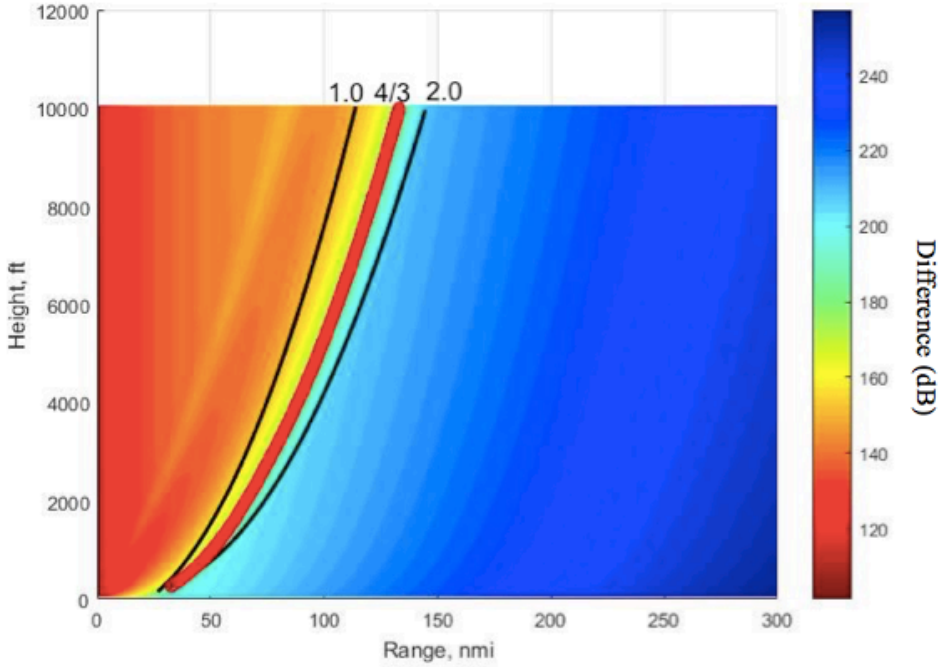

Figure 17. Gradient of Propagation Losses Curves. Baseline 1.0, 4/3, 2.0 in Black and Processed Data in Red

E. CHAPTER SUMMARY

In this chapter, the data collection methodology was introduced. It explained the simulated data collection process employed in this thesis research and the envisaged process using UAVs and other transmitters and receivers of opportunity. The data processing methodology was also discussed. It highlighted the two key functions of the MATLAB codes used for data processing, which are to allow the operator to know immediately whether any atmospheric ducts exist and estimate the value of κ outside the duct. Knowledge of κ allows the operator to choose the optimal system parameters to maximize performance.

In the next chapter, we use the simulated data from AREPS to verify the MATLAB codes for a wider range of scenarios and examine the minimum data requirements for reliable estimates.

IV. SIMULATED TEST RESULTS

Simulated propagation loss data were collected with AREPS using the methodology described in Chapter III. In this chapter, we attempt to verify the MATLAB code's ability to extract the propagation environment under various scenarios. We also examine the minimum data sampling intervals required to allow the code to extract the propagation environment characteristics reliably.

A. METHOD TO DETERMINE THE EXISTENCE OF DUCTS

The first function of the MATLAB code is to calculate and compare the differences between the experimental propagation loss data for an unknown atmospheric condition with propagation losses for known conditions and aims to detect the presence of atmospheric ducts. The simulated data were collected using parameters shown in Table 1.

1. Verifying Capability to Detect Surface Ducts

Two profiles of environmental data files with surface ducts with heights of 500 ft and 1000 ft were created in AREPS. Using the parameters in Table 1, we generated propagation loss data from AREPS using the two profiles and, thereafter, processed the data using the MATLAB code to detect the presence of the surface ducts.

The processed results from propagation loss data of the 500 ft height surface duct are shown in Figure 18. From the processed results, we can clearly observe the presence of surface ducts as well as their ceiling heights.

The result after comparing the differences in propagation loss between the collected data and the known profile is depicted in Figure 18a, and the result after taking the average variation or differences at each height for a range of 300 nmi is shown in Figure 18b. In other words, for Figure 18b we observe that the variations are the largest between 0 to 500 ft, which corresponds to the actual height of the surface duct. The results from propagation loss of the 1000 ft height surface duct yield similar results, and we can clearly observe the presence of the surface duct as well as its height, as seen in Figure 19.

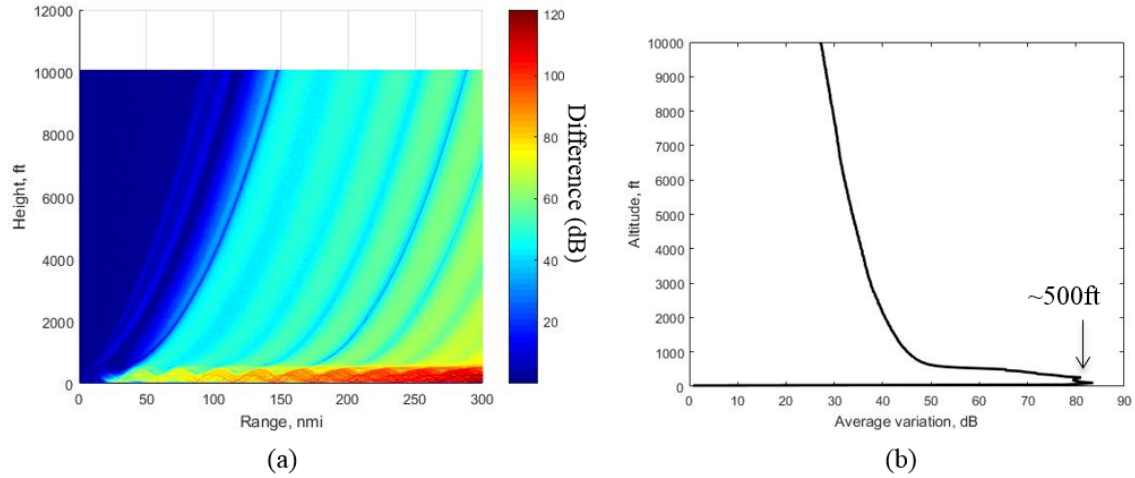

Figure 18. Processed Results Showing a 500-ft Surface Duct. (a) Propagation Loss Difference and (b) Average Variation over Range at Each Height for a Range of 300 nmi.

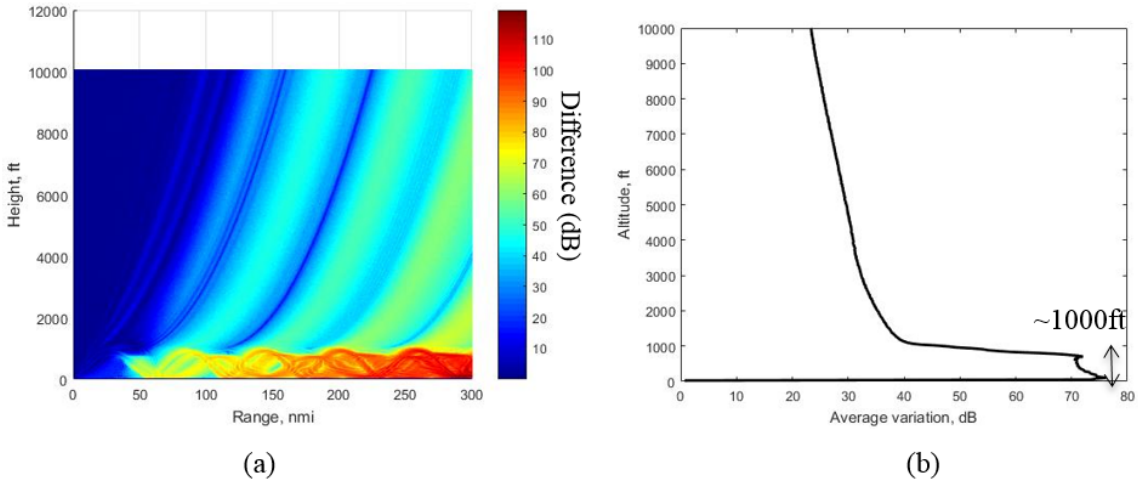

Figure 19. Processed Results Showing a 1000-ft Surface Duct. (a) Propagation Loss Difference and (b) Average Variation over Range at Each Height for a Range of 300 nmi.

2. Verifying Capability to Detect Elevated Ducts

Using AREPS, we created three environment profiles with elevated ducts. Their ceiling and floor heights are summarized in Table 2. .

Table 2. Ceiling and Floor Altitudes of Elevated Duct Profiles

Profile	Elevated Duct Ceiling	Elevated Duct Floor
1.	2000 ft	1580 ft
2.	3500 ft	2950 ft
3.	6100 ft	4080 ft

Using the parameters in Table 1, we generated the propagation loss data from AREPS using the three profiles from Table 2, and the data were processed to detect the presence of the elevated ducts.

From the processed results, we were able to positively identify the presence of the elevated ducts as well as their approximate ceiling and floor heights for all three profiles. The processed results from propagation loss data of profile 1, profile 2, and profile 3 are shown in Figure 20, Figure 21, and Figure 22, respectively. Similar to the preceding section, the (a) figures on the left show the results after comparing the difference in propagation losses between the collected data and the known data. The (b) figures on the right depict the result after taking the average variation or differences at each altitude for a range of 300 nmi. The processed results matched all three profiles very accurately in terms of the ceiling and floor heights. Most importantly, these data were collected with the emitter at 10 ft, which is much lower than the height of the elevated ducts. This proves the capability to detect elevated ducts quite accurately with the emitter located near to the ground.

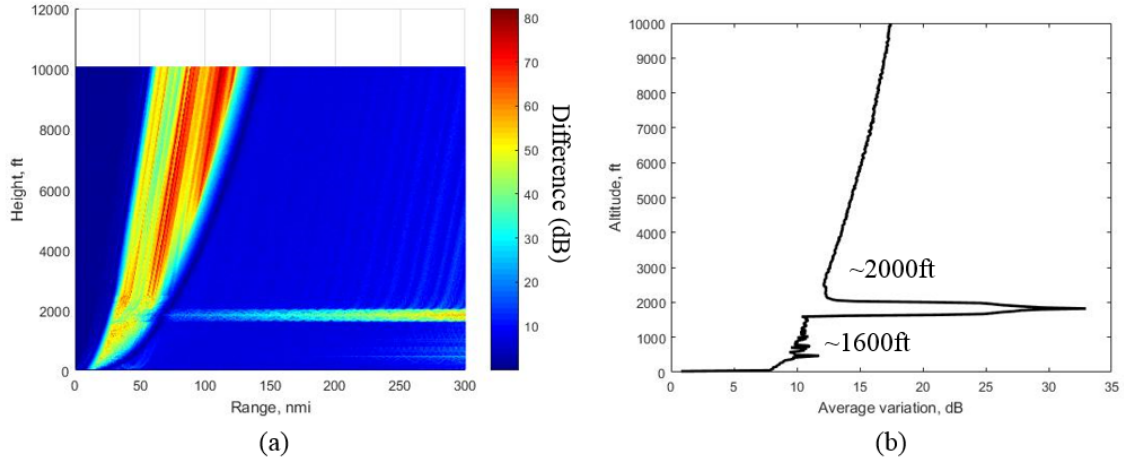

Figure 20. Processed Results Showing a 2000 ft Ceiling Elevated Duct. (a) Propagation Loss Difference and (b) Average Variation over Range at Each Height for a Range of 300 nmi.

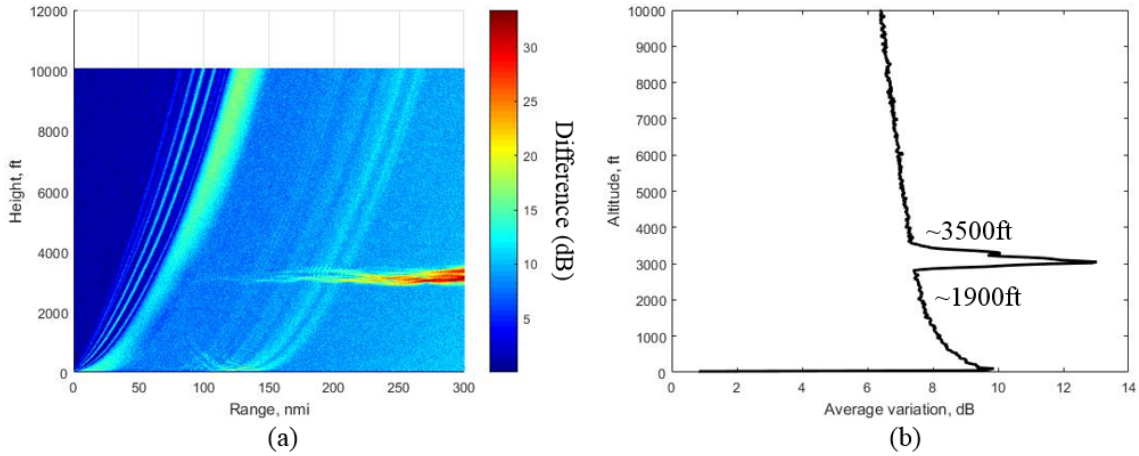

Figure 21. Processed Results Showing a 3500 ft Ceiling Elevated Duct. (a) Propagation Loss Difference and (b) Average Variation over Range at Each Height for a Range of 300 nmi.

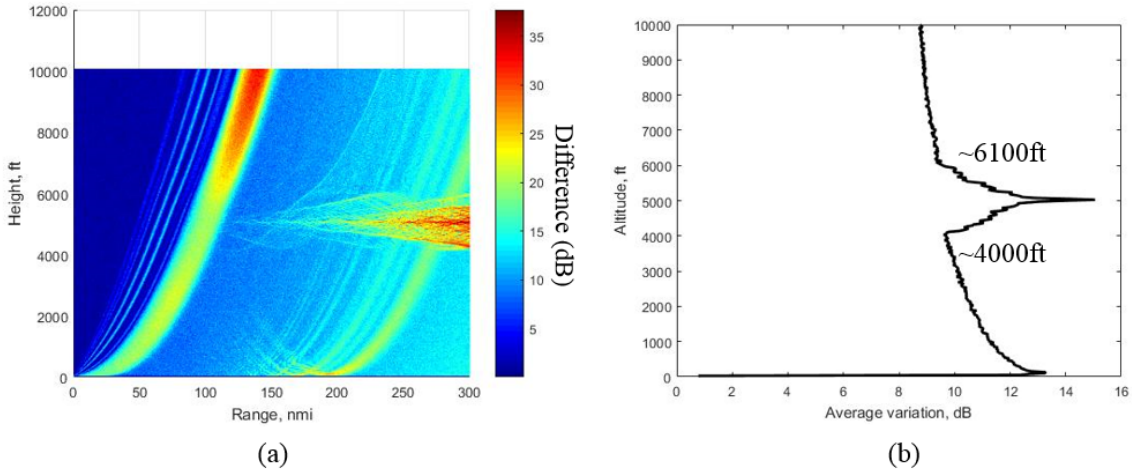

Figure 22. Processed Results Showing a 6100 ft Ceiling Elevated Duct. (a) Propagation Loss Difference and (b) Average Variation over Range at Each Height for a Range of 300 nmi.

3. Minimum Data Points

The data collected in the previous two sections were based on parameters from Table 1 with 384 height output points (N_h) and 440 range output points (N_r) for a total of 168,960 data points over 300 nmi in range and 10,000 ft in height. In reality, it is not possible to collect such a large number of data points over vast distances within a reasonable amount of time; therefore, we attempted to investigate the minimum number of data points over the shortest range and minimum height that still allows the MATLAB code to provide accurate results. To do this, we ran many simulations, gradually reducing the number of output points as well as the height and range from the emitter. The selected profiles-of-interest with their reduced data output points are shown in Table 3. .

From our simulations, we observed that the height output has little consequence to the code's ability to determine the existence of the atmospheric duct, except that it must be higher than the ceiling of the ducts and some data points must exist inside the duct. Therefore, we have chosen 3000 ft for our simulations as the typical ceiling height of the surface duct is below 1000 ft and the ceiling height for elevated duct is usually below 3000 ft [17], [18].

Table 3. Selected Profiles of Interest

Profile	Range (nmi)	No. of Range Outputs (N_r)	Height (ft)	No. of Height Outputs (N_h)
1.	100	400	3000	30
2.	50	20	3000	30
3.	50	5	3000	30
4.	40	4	3000	300

a. Surface Ducts

The propagation loss data for the four profiles in Table 3 were simulated using the environmental data of a surface duct with a height of 1000 ft. The data were then processed to detect the presence of surface ducts. The results for the four profiles are presented in Figure 23 to Figure 26, respectively.

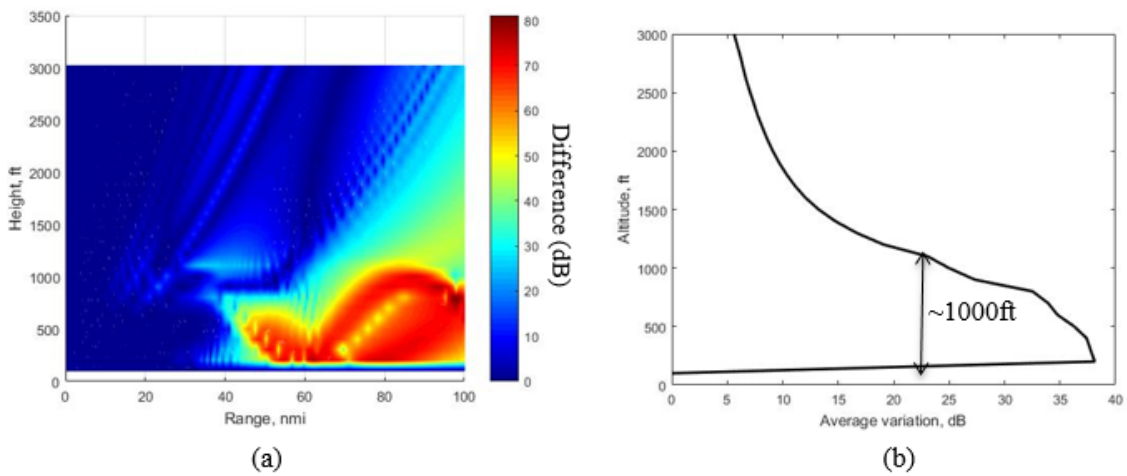

Figure 23. Processed Results of Profile 1 of Table 3 with a 1000-ft Height Surface Duct. (a) Propagation Loss Difference and (b) Average Variation over Range at Each Height for a Range of 100 nmi.

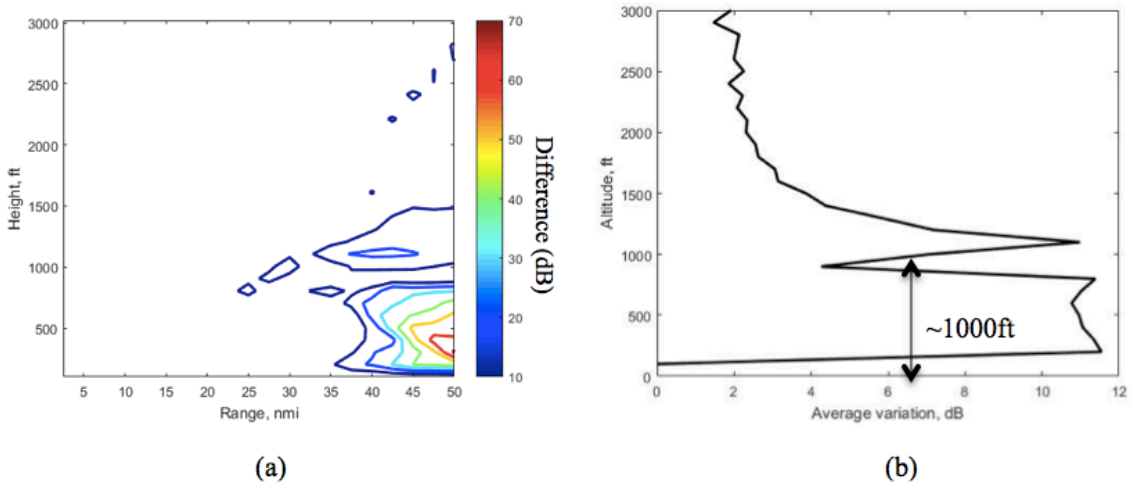

Figure 24. Processed Results of Profile 2 of Table 3 with a 1000-ft Height Surface Duct. (a) Propagation Loss Difference and (b) Average Variation over Range at Each Height for a Range of 50 nmi.

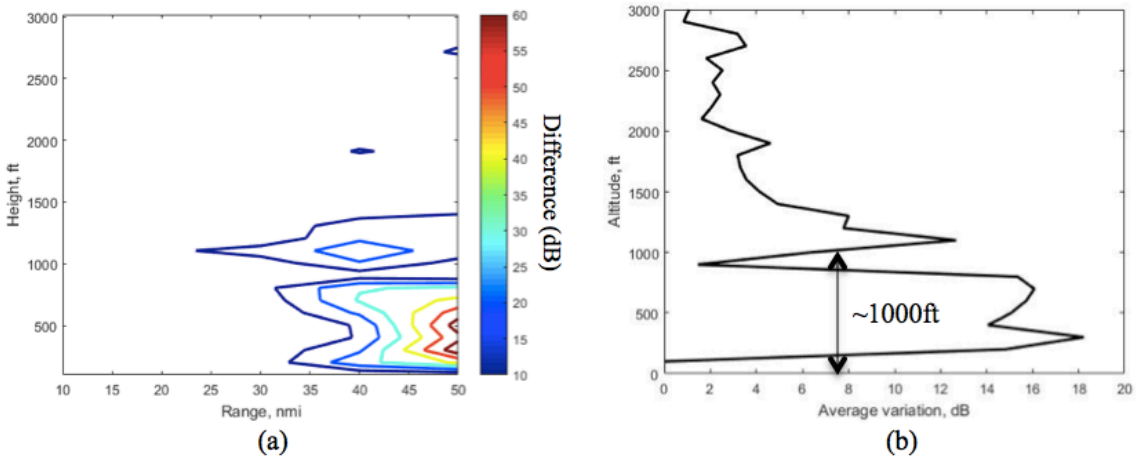

Figure 25. Processed Results of Profile 3 of Table 3 with a 1000-ft Height Surface Duct. (a) Propagation Loss Difference and (b) Average Variation over Range at Each Height for a Range of 50 nmi..

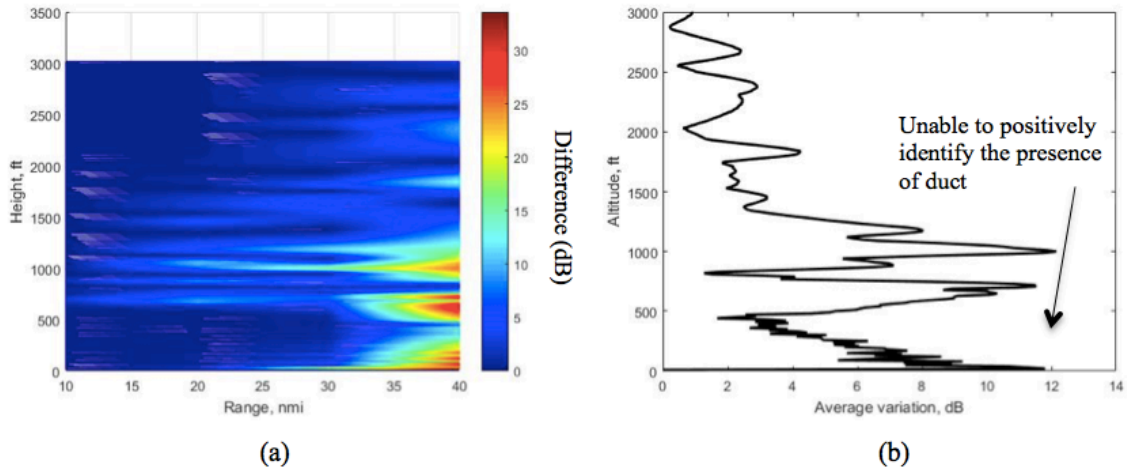

Figure 26. Processed Results of Profile 4 of Table 3 with a 1000-ft Height Surface Duct. (a) Propagation Loss Difference and (b) Average Variation over Range at Each Height for a Range of 40 nmi.

There are two observations that were gleaned from the results. Firstly, by comparing the (a) figures on the left (Figure 23 to Figure 26), we observe that the results are not clear when the data points were fewer than 1000 (i.e., Figure 24a and Figure 25a).

Secondly, we were still able to observe the presence of the 1000 ft height surface duct in Figure 23b, Figure 24b, and Figure 25b even though the resolution is not as clear as in Figure 19, which had 168,960 data points. We were not able to positively identify the surface duct when the range was reduced to 40 nmi in Figure 26. This is because the wave paths only start to behave differently in the surface duct as compared to standard atmospheric conditions when they are about 40 nmi away from the emitter as shown in Figure 27; therefore, we are able to conclude that 50 nmi is the minimum range required to detect surface ducts in this case. As a result, we can reduce the number of range output points to five (i.e., one data point every 10 nmi) if we are using only "average variations" as the means to detect surface ducts using the (b) figures on the right.

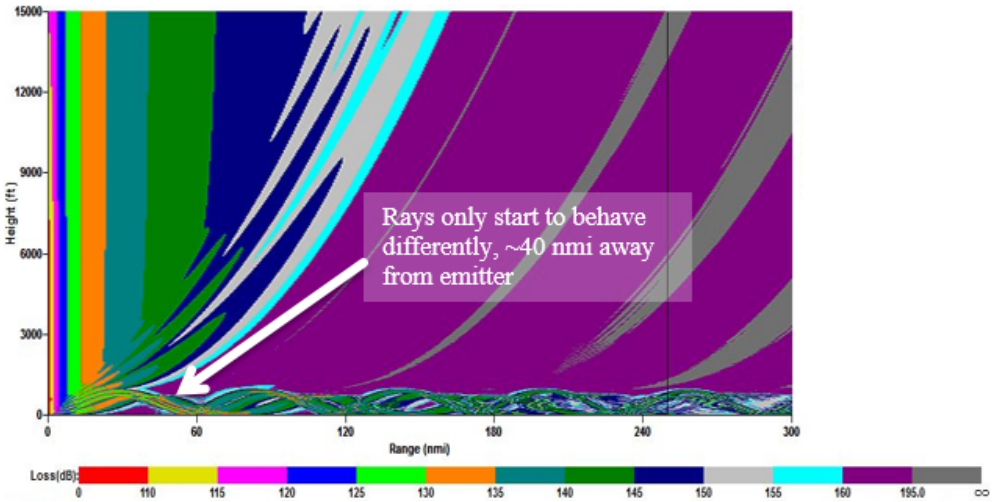

Figure 27. Propagation Loss Data from AREPS in 1000-ft Height Surface Duct

b. Elevated Ducts

The propagation loss data for the four profiles in Table 3 were simulated for an elevated duct with ceiling height of 2000 ft (Profile 1 of Table 2). The data were then processed to detect the presence of the elevated ducts. The results for the four profiles are presented in Figure 28 to Figure 31.

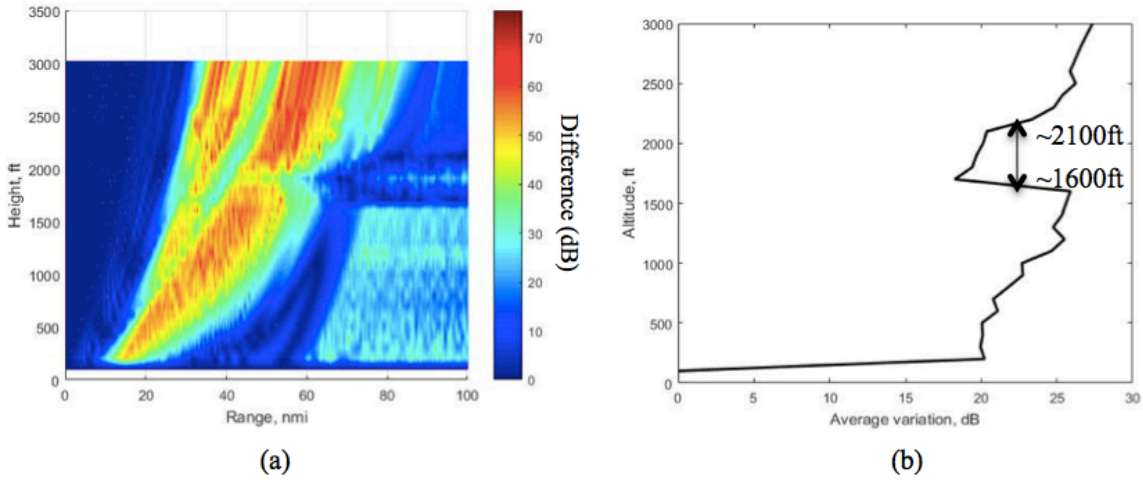

Figure 28. Processed Results of Profile 1 of Table 3 with a 2000-ft Ceiling Elevated Duct. (a) Propagation Loss Difference and (b) Average Variation over Range at Each Height for a Range of 100 nmi.

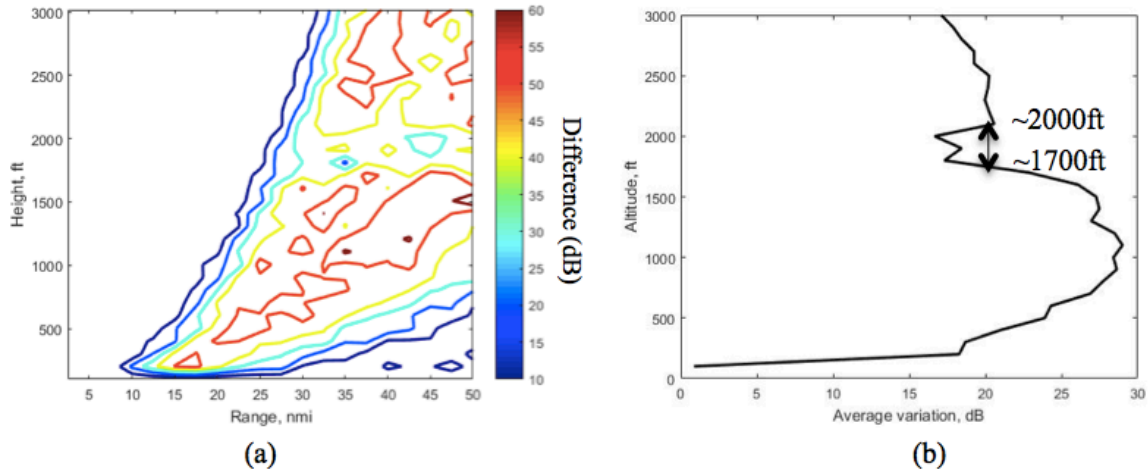

Figure 29. Processed Results of Profile 2 of Table 3 with a 2000-ft Ceiling Elevated Duct. (a) Propagation Loss Difference and (b) Average Variation over Range at Each Height for a Range of 50 nmi

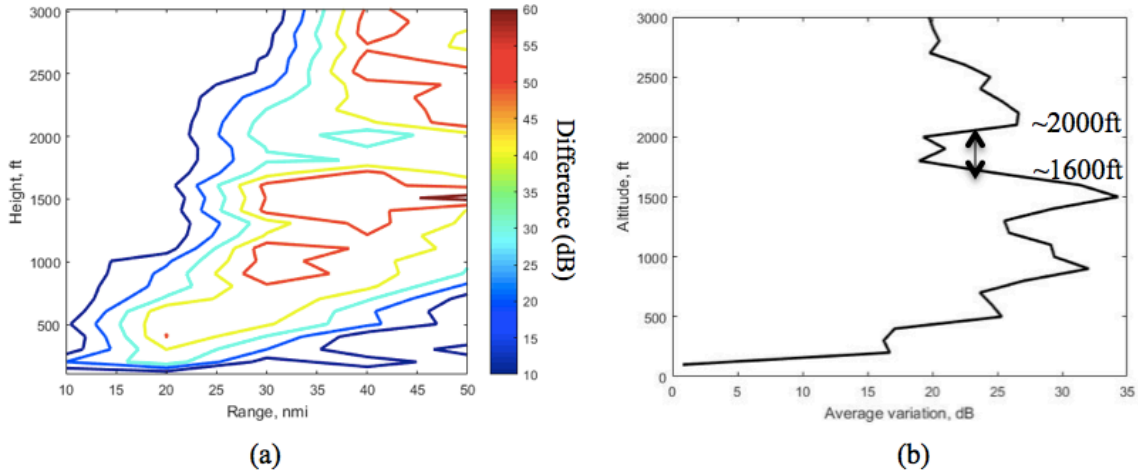

Figure 30. Processed Results of Profile 3 of Table 3 with a 2000-ft Ceiling Elevated Duct. (a) Propagation Loss Difference and (b) Average Variation over Range at Each Height for a Range of 50 nmi.

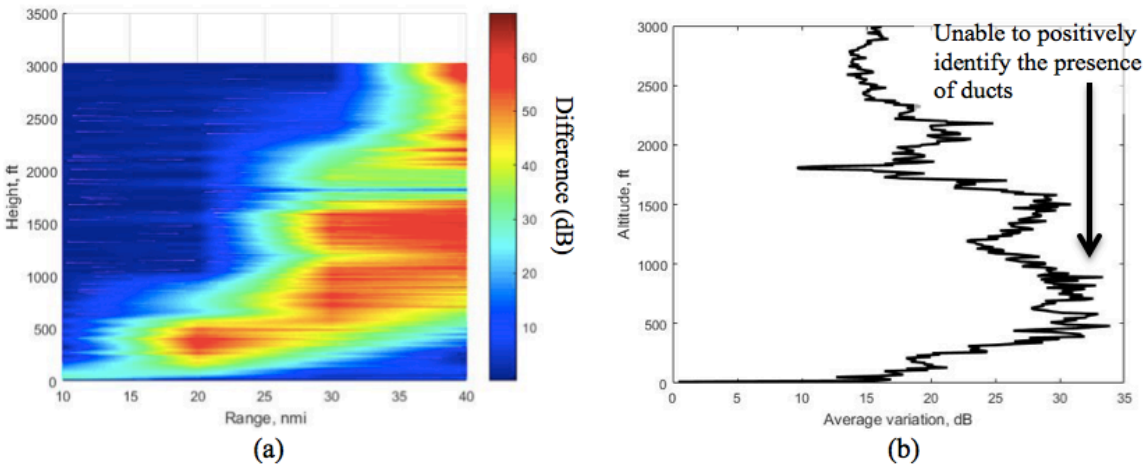

Figure 31. Processed Results of Profile 4 of Table 3 with a 2000-ft Ceiling Elevated Duct. (a) Propagation Loss Difference and (b) Average Variation over Range at Each Height for a Range of 40 nmi.

There are a few observations gleaned from the results:

1. The results from the (a) figures on the left are not as clear when the data points are fewer than 1000 (similar to our earlier observation for the surface duct); nevertheless, the presence of the elevated duct at 2000 ft is somewhat visible in all four profiles.

2. From the (b) figures on the right, we see that average variations are the lowest at altitudes corresponding to the elevated ducts. The resolution is still relatively good up to profile 3, where the range is up to 50 nmi. The result is not so clear when the range is reduced to 40 nmi (similar to the observation for the surface duct).

3. The (b) figures on the right indicate the existence of elevated ducts when the average variations are the lowest. This is different from Figure 20 to Figure 22 where the average variations are the highest inside elevation ducts. This is because the results from Figure 20 to Figure 22 were based on data up to 300 nmi, whereas the results from Figure 28 to Figure 31 were based on data between 50 nmi to 100 nmi.

4. At far range (more than 100 nmi), the propagation loss is smaller inside the elevated ducts due to the trapping phenomenon as compared to standard conditions where almost all the signals were lost at such distances from the emitter; therefore, we get high propagation loss variations at altitudes corresponding to the elevated ducts.

5. For near range (less than 100 nmi), the effect of variations is stronger at areas below the elevated ducts. The presence of elevated ducts causes the rays to bend upwards and results in higher propagation loss than normal at regions under the elevated ducts. This phenomenon is illustrated in Figure 32.

6. In the diagram in Figure 32a, we see the propagation loss for standard conditions, and in Figure 32b, we see the propagation loss when there is an elevated duct at 2000 ft. In Figure 32c, we see the processed result after comparing the two data sets. The red circles indicate the regions where the elevated duct causes the electromagnetic rays to bend upwards and result in high propagation losses as compared to standard conditions. This could result in loss of detection capability (missed targets).

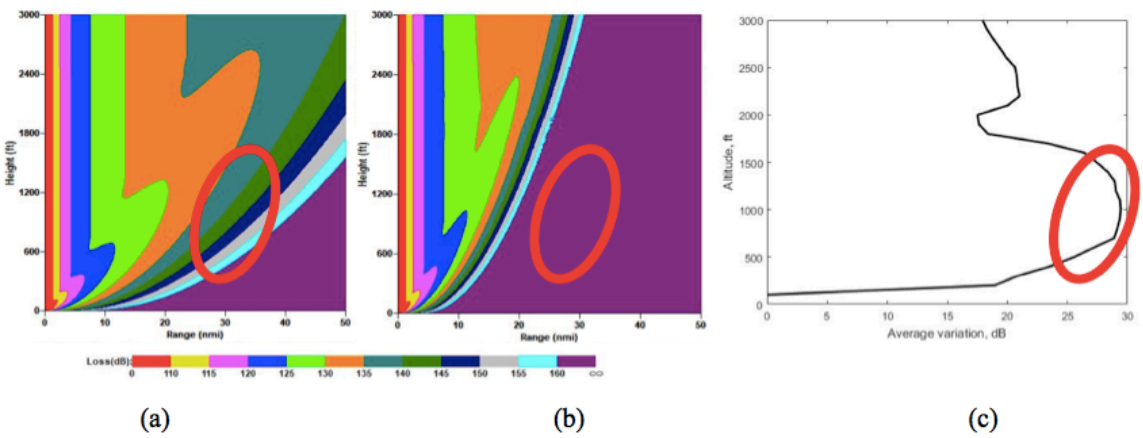

Figure 32. (a) Propagation Loss in Standard Conditions, (b) Propagation Loss when 2000 ft Elevated Duct is Present, (c) Average Variations from Comparing both Data

c. Minimum Data Points

From the results described earlier, it appears that 50 nmi is the minimum range required to ascertain the existence of both surface and elevated ducts. The data points in the horizontal range direction could be reduced to five (i.e., one data point per 10 nmi) and still achieve good results if we are using only average variation to determine the existence of ducts. Note that we have assumed that the ducts extend large distances in range, which rarely is the case.

The minimum height is approximately 3000 ft or dependent on the height of the typical elevated ducts in the environment-of-interest. The minimum height to collect the data must exceed the height of the elevated ducts, and some data points must be inside the duct. The minimum data in the vertical height direction is one data point per 100 ft. The suggested minimum data points are summarized in Table 4. . For example, to scan an area of 50 nmi up to 3000 ft, we require a minimum of five data points in the horizontal range direction and 30 data points in the vertical height direction, which works out to a total of 150 data points. This is the absolute minimum required assuming high receiver sensitivity.

Table 4. Minimum Data Points for the Cases Investigated

	Parameters
Minimum Range	50 nmi
Minimum Data Points in Horizontal Direction, N_r	1 data point per 10 nmi
Minimum Height	Higher than typical ceiling height of elevated duct
Minimum Data Points in Vertical Direction, N_h	1 data point per 100 ft

B. METHOD TO DETERMINE THE κ VALUE

The second function of the MATLAB code is to determine the value of κ. The code calculates the range R at which a reference signal strength occurs at each height h. The particular reference is not important but must be above the reliable measurement threshold for all ranges. The resulting (h, R) data are then fitted into a gradient curve

using the MATLAB "polyfit" function. The baseline gradient curves for $\kappa = 1.0$, $\kappa = 4/3$, and $\kappa = 2.0$ are superimposed on the contour plot as shown in Figure 33. The MATLAB code plots the gradient curve and matches it to the closest baseline gradient curve using numerical calculations such as least squares to match the data to the baseline gradients.

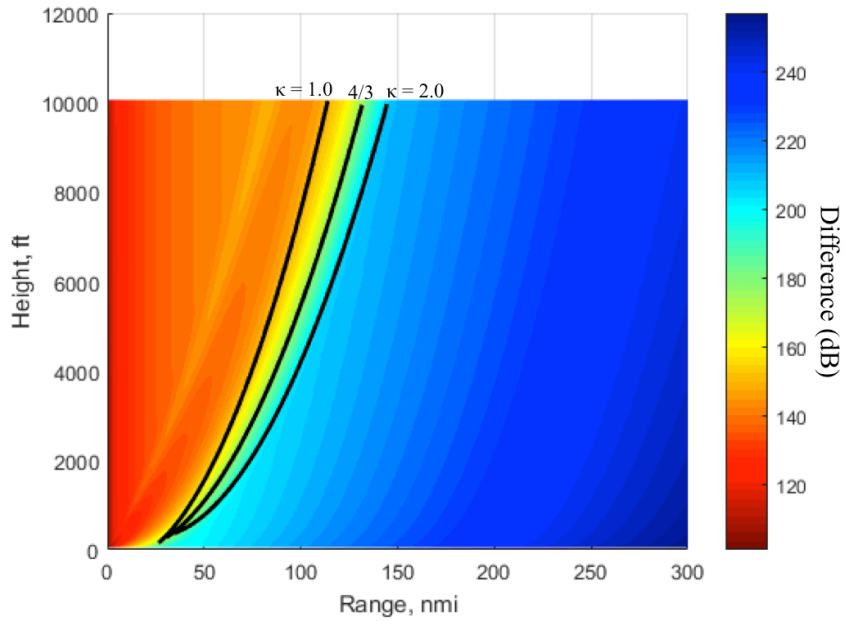

Figure 33. Baseline Gradient Curves for $\kappa = 1.0$, $\kappa = 4/3$, and $\kappa = 2.0$

1. Verifying the Capability to Estimate κ Value

Environmental files with various κ values were created in AREPS to simulate the atmospheric conditions. Using the parameters in Table 1, we generated the propagation loss data from AREPS and processed it using the MATLAB code to derive the gradient curves and then compare the curve fits to the baseline curves.

The data curve fits were able to match the baseline gradient curves accurately. For example, the gradient curve from AREPS contours for $\kappa = 1.0$ is shown as circles in Figure 34 and overlap the $\kappa = 1.0$ baseline curve. Similarly, the gradient curves from AREPS contours for $\kappa = 4/3$ and $\kappa = 2.0$ are shown in Figure 35 and Figure 36, respectively. As

seen from Figure 34, Figure 35, and Figure 36, the calculated gradients correctly matched the gradient of the baseline curves.

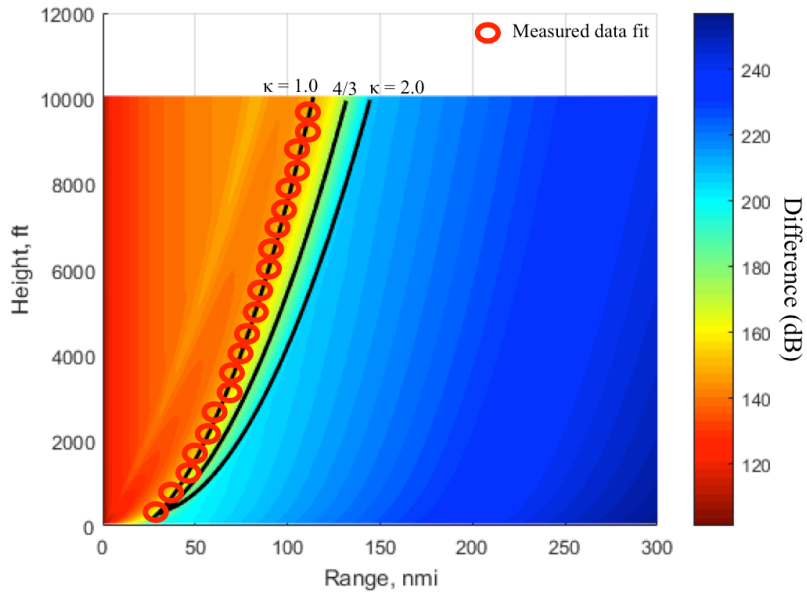

Figure 34. Results of Gradient Curve for $\kappa = 1.0$ Based on AREPS $\kappa = 1$ Data

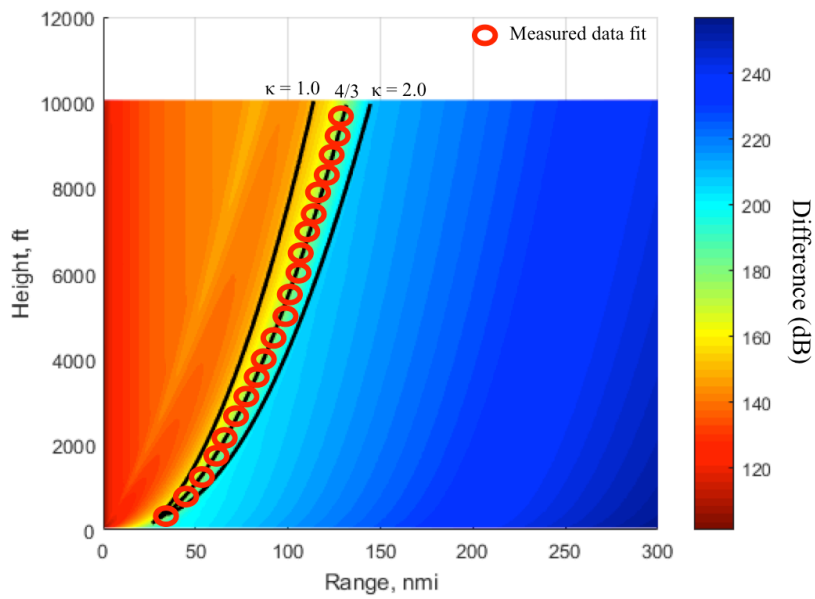

Figure 35. Results of Gradient Curves for $\kappa = 4/3$ Based on AREPS $\kappa = 4/3$ Data

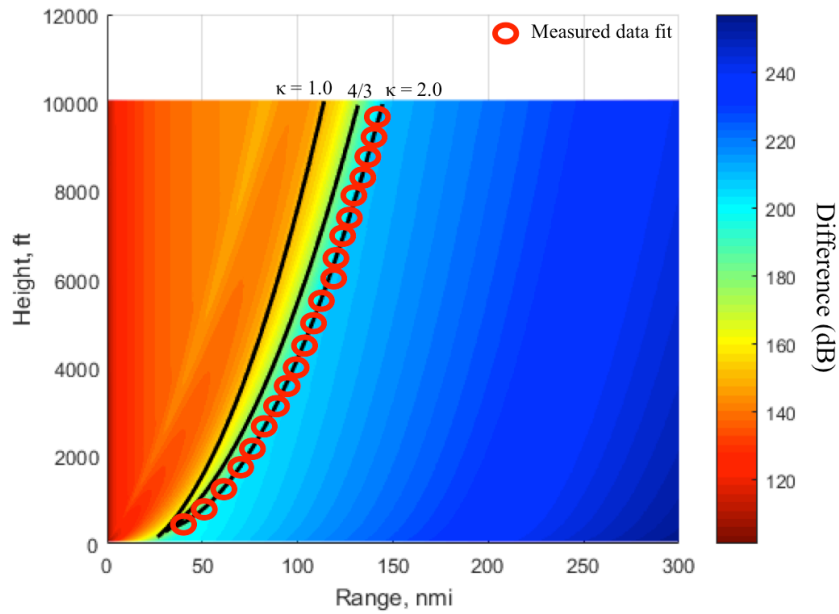

Figure 36. Results of Gradient Curves for $\kappa = 2$ Based on AREPS $\kappa = 2$ Data

2. Minimum Data Points

The previously discussed simulations were conducted based on the AREPS default setup as shown in Table 5. . To determine the minimum number of data points required, the range, height, and sampling distances were gradually reduced. Simulations were run to check whether the procedure still generate the proper gradient curves. After running the simulations, we observed that a minimum horizontal range of 125 nmi with 100 data points is required to allow the code to fit the results to the proper gradient curves. For a height of 3000 ft, 30 data points are required to allow the code to fit the results into gradient curves. Poor results from using 50 nmi range and 100 nmi range are shown in Figure 37. The code was unable to fit the results into smooth gradient curves due to lack of data. In Figure 38, the range was extended to 125 nmi, and the code was able to fit the gradient curve that is somewhat smooth; therefore, based on the existing code's fitting method, the minimum range required to predict the value of κ is about 125 nmi. A more complex fitting method needs to be applied to reduce the minimum range.

Table 5. Default Simulation Setup

	Parameters
Range	300 nmi
Data Points in Horizontal Direction, N_r	440
Height	10,000 ft
Data Points in Vertical Direction, N_h	384

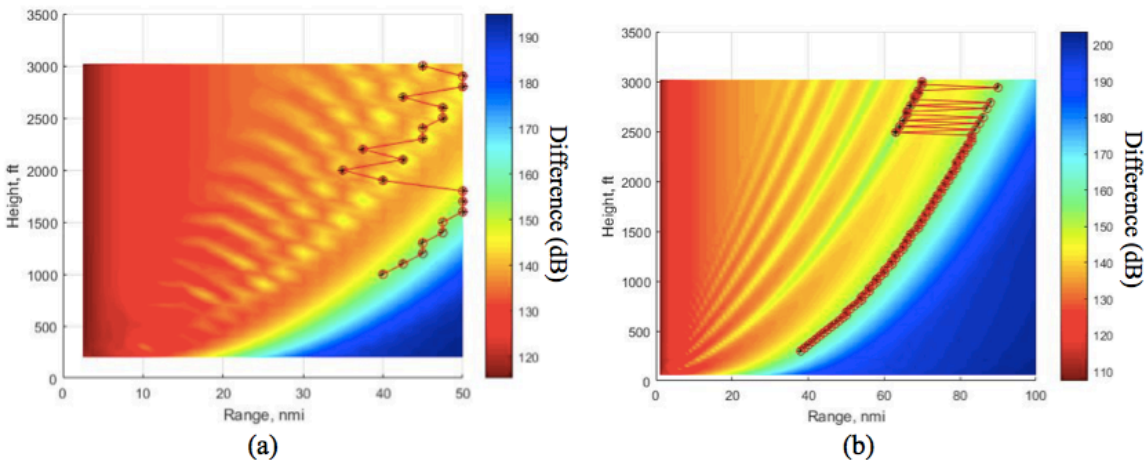

Figure 37. Unable to Fit Gradient Curves for (a) 50 nmi Range and (b) 100 nmi Range

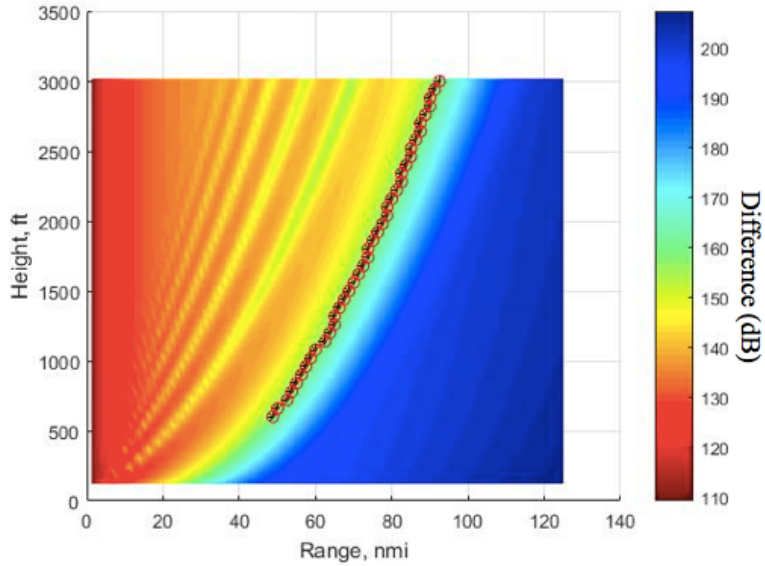

Figure 38. Gradient Curve for 125 nmi Range

As compared to a duct, finding κ requires a much larger range (125 nmi) as well as more data points (100 in horizontal range direction). The need to collect more than twice the data and the greater range increases the time required to collect the data as compared to duct sensing. The summarized results are presented in Table 6. .

Table 6. Minimum Samples Requirement for Both Functions

	Duct Sensing	**κ-estimate**
Range	50 nmi	125 nmi
Min. Data Points in Horizontal Direction	5	100
Height	3,000 ft	3,000 ft
Min. Data Points in Vertical Direction	30	30
Total Data Points	150	3000

C. CHAPTER SUMMARY

In this chapter, we verified the capability of the algorithm and software to determine the presence of both surface and elevated ducts. We also verified the capability to determine the κ value by comparing the gradient curves to the baseline curves. The minimum number of data points to achieve these capabilities was also examined. In the next chapter, we investigate the system implementation requirements.

THIS PAGE INTENTIONALLY LEFT BLANK

V. SYSTEM IMPLEMENTATION REQUIREMENTS

In this chapter, we present the basic architecture of the overall envisaged system to collect and process the propagation loss data. We investigate some of the system requirements such as frequency spectrum, receiver sensitivity, and the associated transmitter power as well as supporting equipment such as the global positioning system (GPS) and data link for transfer of data. We also examine the total time required to collect sufficient data based on a collection pattern and the number of UAVs available.

A. SYSTEM DIAGRAM

The envisaged system to collect and process the propagation loss data is illustrated in Figure 39. To start, we consider an emitter on board a ship that transmits a signal and UAVs that measure the signal power with reference to their positions from the emitter. It is also possible to use emitters of opportunity from shored-based transmitters or other UAVs fitted with compatible emitters. The measured data is sent back to the processing computer on the ship, which calculates the propagation losses with respect to a common location. The computer calculates and compares the propagation loss data against that of the baseline conditions to determine κ and if any atmospheric ducts exist. To achieve this, the UAVs require the following onboard equipment:

1. Receiver—to measure signal power
2. GPS—to determine the accurate location when measuring signal power
3. Altimeter—to determine the accurate height when measuring signal power
4. Gyroscopic instruments—to determine polarization and gain losses due to pointing direction of the antenna
5. Data storage and local processing capability—to store and process signal power, location, and height data
6. Data link—to send data to processing computer

The key functions of each element onboard the UAVs as well as those onboard the ship are shown as a block diagram in Figure 40 and described in Table 7. .

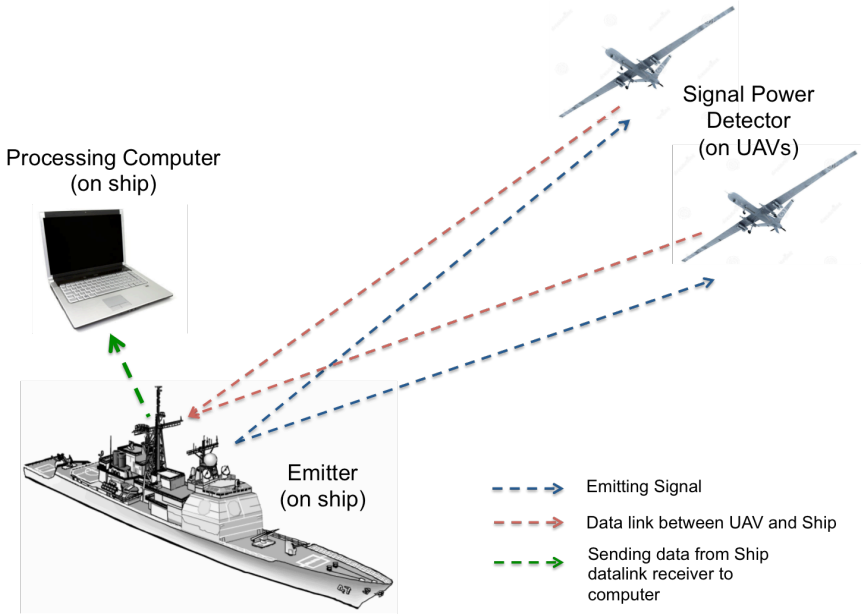

Figure 39. Envisaged System to Collect and Process Propagation Loss Data

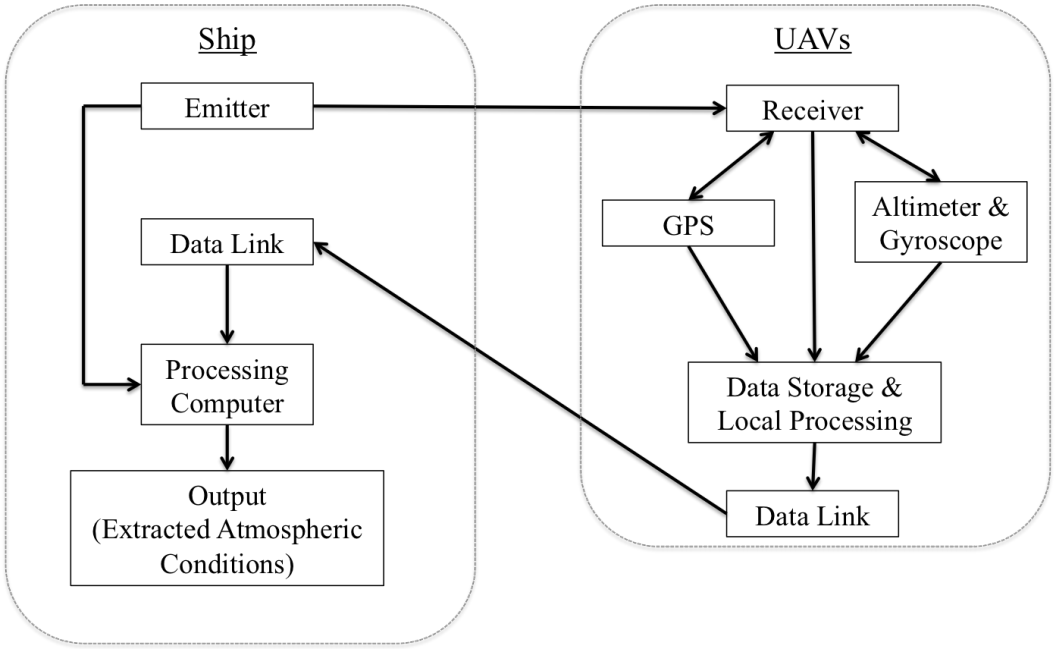

Figure 40. Block Diagram of Equipment for Data Collection and Processing

Table 7. Key Functions of Envisaged System

Type	Location	Key Function	Details
Emitter	Ship	Transmit Signal	• Transmit signal at known frequency and power
Receiver	UAV	Collect Data	• Measure signal power
GPS	UAV	Collect Data	• Determine GPS timing and location during sampling
Altimeter	UAV	Collect Data	• Determine height during sampling
Gyroscope	UAV	Collect Data	• Determine the azimuth and elevation angles of the antenna
Hard Disk	UAV	Store Data	• Store signal power, location, and height information • Provide local processing power
Data-link between UAV and Ship	Ship/ UAV	Send Data to Ship	• Send data of signal power with GPS locations, height, and timing to processing computer
Processing Computer	Ship	Process Data	• Correlate data with emitter location to determine propagation losses with respect to height and range from emitter (ship is moving) • Determine if duct exists • Determine κ value • Calculate radar horizon given κ value • Calculate electromagnetic emission range given existence of duct

B. FREQUENCY SELECTION

In this section, we investigate the several frequencies for the systems to operate. Studies have shown that the attenuation of signals increases with increasing frequencies [10]; therefore, as the frequency of the signal increases, propagation losses also increase. In Figure 41, we observe that the propagation losses increase with increasing frequencies. Another consideration is that the effects of ducting are more pronounced at certain frequencies. Finally, the primary frequencies of interest are those of the systems operating onboard the ships; therefore, the selection of operating frequency is important.

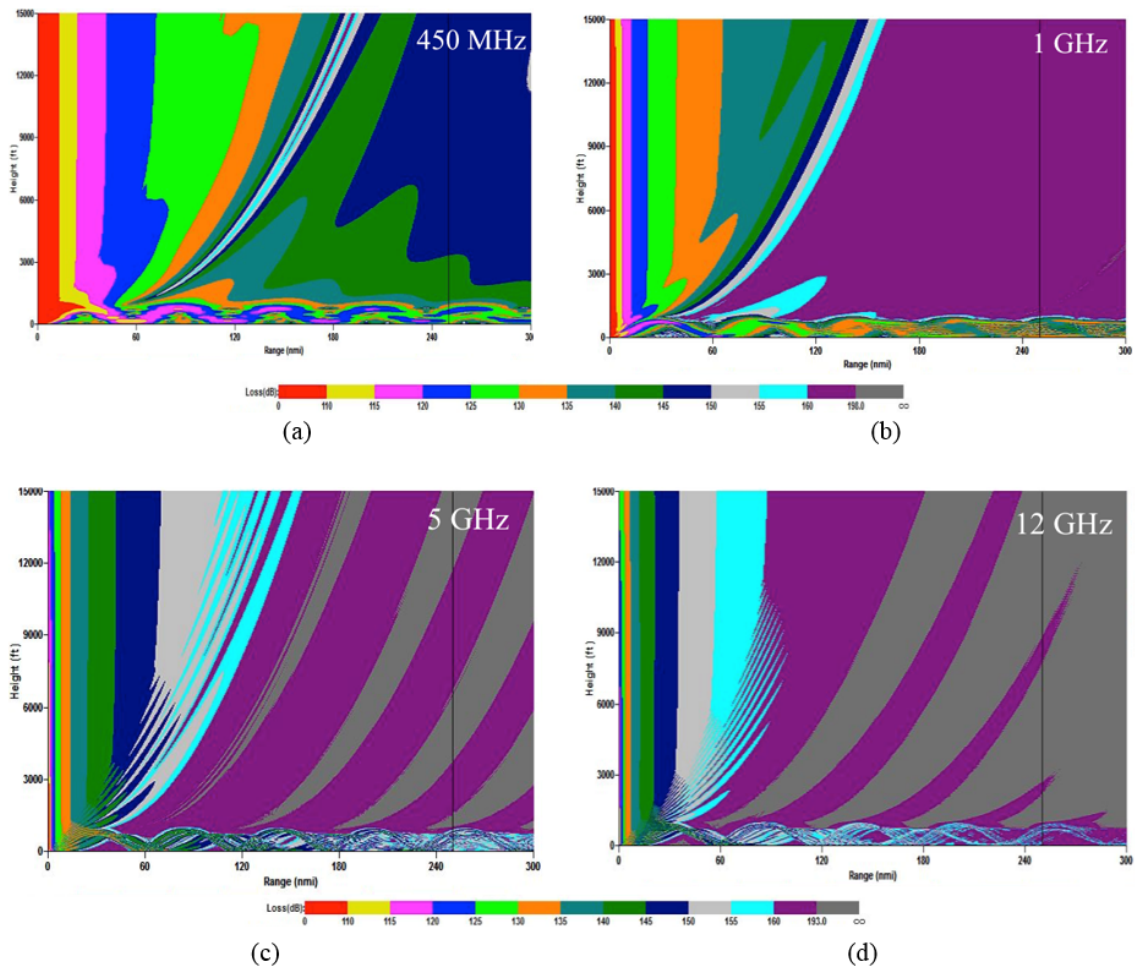

Figure 41. Propagation Losses for (a) 450 MHz, (b) 1 GHz, (c) 5 GHz, and (d) 12 GHz

During the course of the simulation studies (between 450 MHz and 12 GHz), we observed that it may not be suitable to use low frequencies (HF, VHF, and UHF) as the propagation losses or attenuation are too low; therefore, the compared differences may be too close between the unknown (i.e., the environment of interest) and known baseline conditions. Such a case would be very susceptible to measurement errors. As such, we conducted simulations by varying the frequencies of the emitter (450 MHz, 1 GHz, 3 GHz, 5 GHz, 7 GHz, and 12 GHz) with the parameters shown in Table 8. . The processed results from the MATLAB code for a surface duct environment are shown in Figure 42, and the results for an elevated duct environment are shown in Figure 43.

Table 8. Parameters Used for Data Collection

	Type / Parameters
Peak Power	2000 kW
Pulse Length	9 μs
Receiver Noise Figure	5.5 dB
Assumed System Loss	3 dB
Maximum Antenna Gain	39 dB
Horizontal Beam Width	2°
Vertical Beam Width	1.5°
Antenna Elevation Angle	0.5°
Antenna Polarization	Horizontal
Antenna Height	10 ft
Range Output Points	5
Height Output Points	30
Range	50 nmi
Height	3000 ft

From Figure 42 and Figure 43, we observe that the results are not clear when the frequency is below 1.0 GHz for both surface duct and elevated duct conditions. The results for elevated duct conditions are not so clear when the frequencies are above 5.0 GHz as they do not show the ceiling and floor heights clearly. The best results occur when the frequency is 3.0 GHz; therefore, it is recommended that the emitter system operate in the 2.0 to 4.0-GHz range (S Band) for the best results.

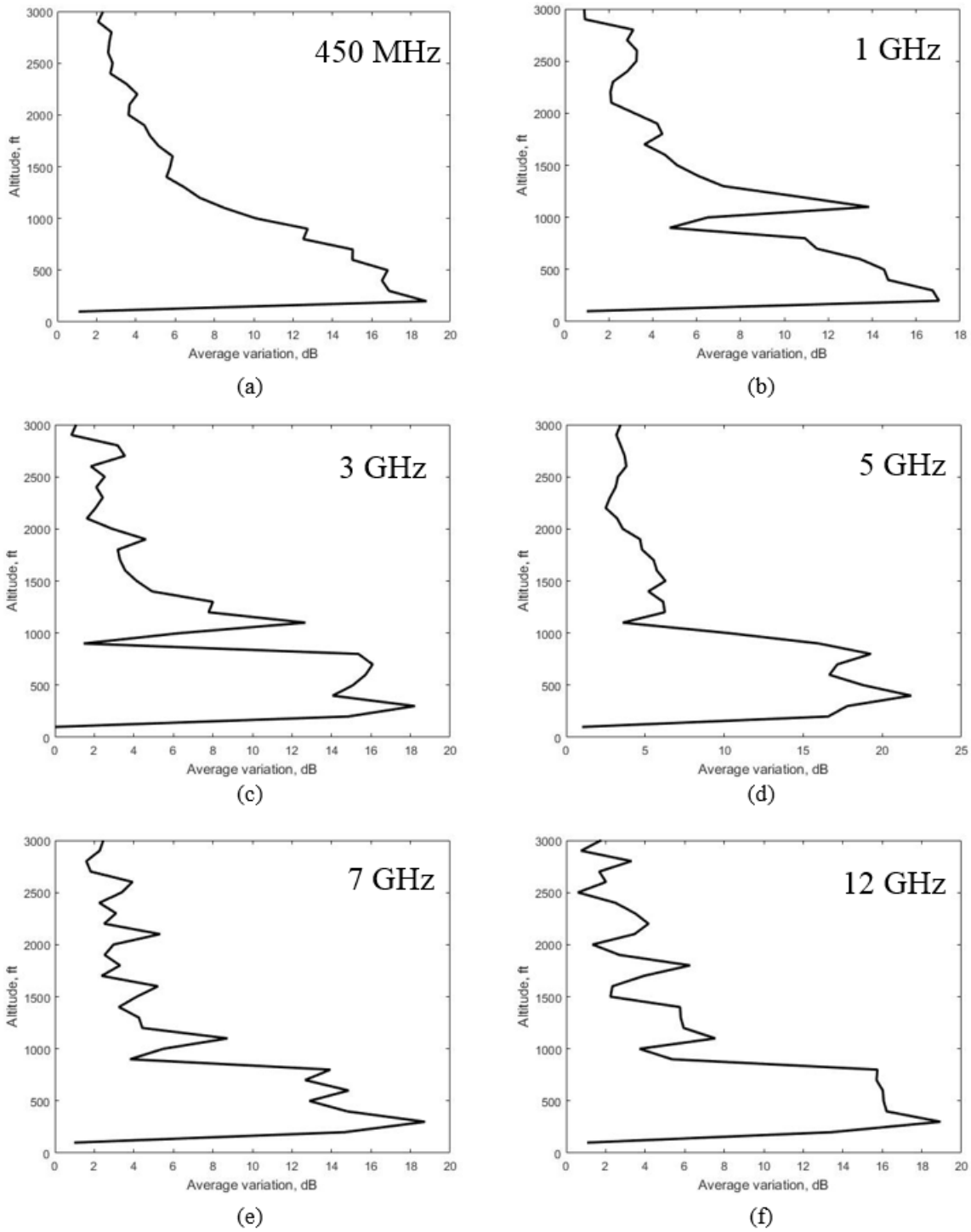

Figure 42. Processed Results to Identify 1000 ft Surface Duct with Frequencies (a) 450 MHz, (b) 1 GHz, (c) 3 GHz, (d) 5 GHz, (e) 7 GHz, and (f) 12 GHz

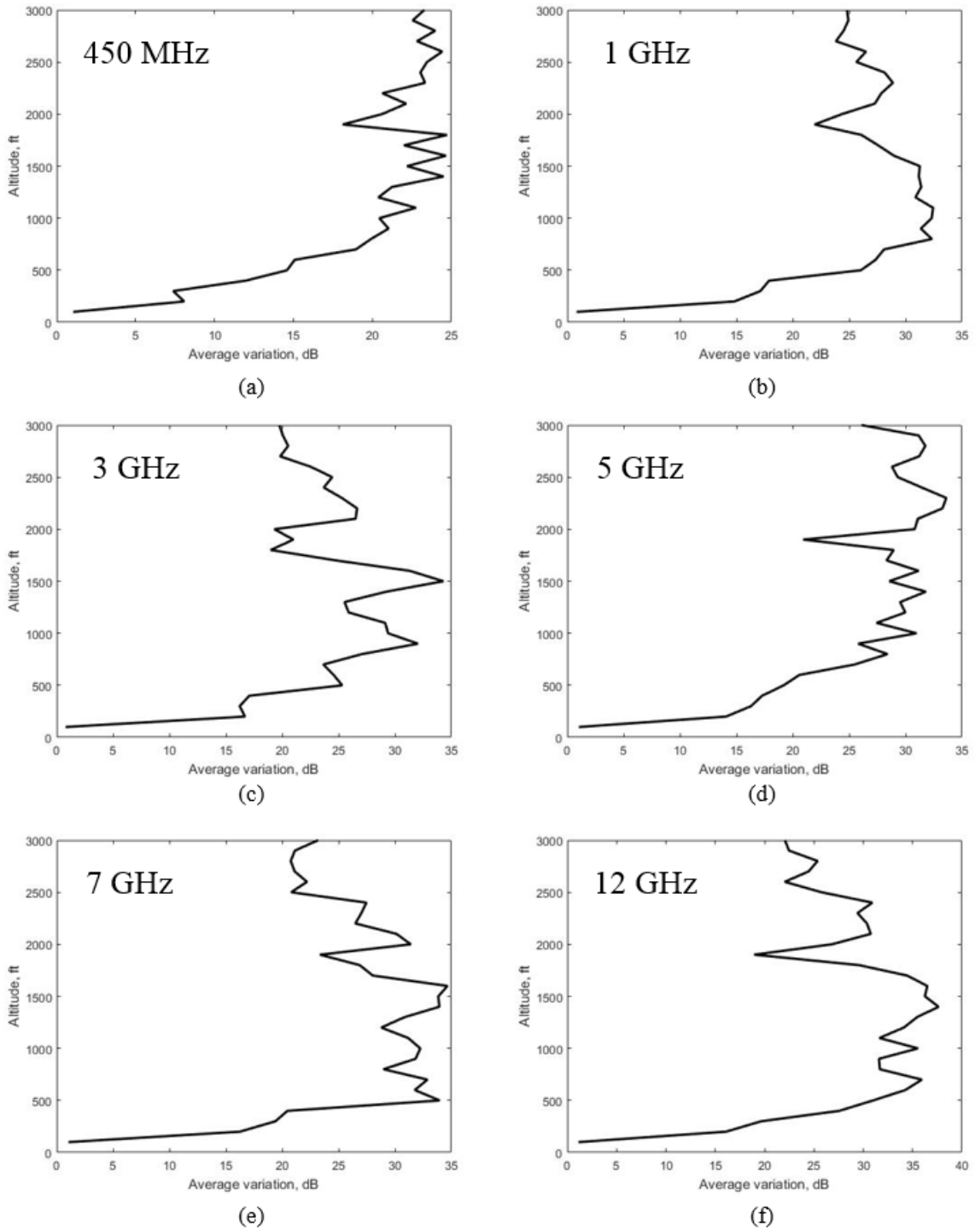

Figure 43. Processed Results to Identify 2000 ft Ceiling Elevated Duct with Frequencies (a) 450 MHz, (b) 1 GHz, (c) 3 GHz, (d) 5 GHz, (e) 7 GHz, and (f) 12 GHz

C. RECEIVER SENSITIVITY AND TRANSMITTER MINIMUM EFFECTIVE ISOTROPIC RADIATED POWER

Receiver sensitivity refers to the ability of a receiver to detect a signal with a power that is above the noise level [19]. In the case of this system, a spectrum analyzer or power detector is mounted on the UAVs to detect the signal levels at the required locations (i.e., up to 125 nmi range and 3000 ft height from the source emitter). Assuming a minimum signal-to-noise ratio (SNR) of 15, we have the minimum discernible signal (MDS)

$$\begin{aligned} \mathrm{MDS}_{\mathrm{dB}} &= \text{noise floor}_{\mathrm{dB}} + \mathrm{SNR}_{\mathrm{dB}} \\ &= \text{noise floor}_{\mathrm{dB}} + 15 \text{ dB}. \end{aligned} \tag{9}$$

In our research on commercially available handheld spectrum analyzers, we found that entry-level spectrum analyzers have an average noise floor of −80 dBm, and high-end professional spectrum analyzers with pre-amplifiers have a much lower average noise floor of −170 dBm [20]. The noise floor of the spectrum analyzer determines how much power the emitter is required to transmit to ensure the receiver is able to detect signal power accurately.

From the AREPS program, we observed that the spectrum analyzer would need to detect propagation loss of up to 160 dB at a distance of 125 nmi for the data processing program to be able to compare the propagation losses effectively; therefore, the minimum effective isotropic radiated power (EIRP) is

$$\mathrm{EIRP}_{\mathrm{dB}} = \mathrm{MDS}_{\mathrm{dB}} - \left(-160 \text{ dB}\right). \tag{10}$$

If a professional handheld spectrum analyzer of average noise level of −145 dBm is used with a SNR of 15, the EIRP required is approximately 1 W to allow accurate extraction of the propagation environment. The EIRP required for spectrum analyzers of different average noise levels is presented in Table 9. .

Table 9. EIRP Required for Various Types of Spectrum Analyzers

Type of Spectrum Analyzers [20]	Average Noise Level (dBm)	EIRP
Entry Level	−80	3.16 MW
Intermediate Level [20]	−90	0.316 MW
Professional Level	−145	1 W
Professional Level with Pre-amplifier	−160	0.0316 W

D. SUPPORTING EQUIPMENT

There is a need for supporting equipment onboard the UAVs and ship for data transfer and processing. The proposed equipment is described in the following paragraphs.

1. GPS, Altimeter, and Gyroscope

To achieve accuracy when measuring propagation loss, we need proper correlation between the transmitted signal and received signal power as the emitter (i.e., onboard ship) could be in motion when the UAVs are measuring received signal power. We also need to know the attitude (i.e., azimuth and elevation) of the receiver so that polarization and pattern losses can be taken into account when calculating propagation losses.

To correlate the data correctly, the measured received signal power must be stamped with highly accurate GPS location, GPS time, altimeter height, and the attitude of the receiver using a gyroscope. This information allows the computer to correlate the data with the location and time of the emitter (i.e., transmitted signal) and determines the propagation loss in terms of range and height from the emitter, taking antenna pointing into consideration.

2. Data Storage and Local Processing Capability

Data consisting of measured received signal power, time-stamped with GPS location, attitude, and altimeter height needs to be stored for the duration of the data collection process. A small amount of local processing power is also required to process this information. As the data size is not expected to be large, modern data storage technologies such as a solid-state drive (SSD) are suitable as they are small and lightweight and can be easily retrofitted into any system.

3. Data Link

For fast data processing, the system can have a data link between the UAVs and the processing computer (possibly located on the ship) for transfer of data instead of having to wait for the UAVs to land before manual transfer of data. This allows the computer to process and update the estimates as more data continues to be collected by the UAVs. It is possible that the data link hardware could be shared with the loss measurement system.

4. Processing Computer

The key function of the processing computer is to use the developed algorithm to determine the existence of duct and κ. It also needs to correlate the data (i.e., the distance between the emitter and receiver). There is no requirement for the computer to have large processing capacity, and a typical workstation desktop or laptop can perform the function.

E. FLIGHT PATTERNS AND DATA COLLECTION TIME

In this study, we assumed that ideally reliable processing requires propagation loss data up to 125 nmi in range and 3000 ft in height from the emitter. This is based on the simulation results described in Chapter IV, where this is the minimum to detect both atmospheric ducts and extract κ. The number of UAVs available, sampling rate, and flight patterns determine the time required to complete the data collection process.

1. Flight Pattern

It is assumed that the atmospheric propagation condition in one radial direction is representative of the propagation condition in the region or environment of interest (i.e., it is independent of azimuth); thus, data is collected in a vertical plane at a fixed compass (azimuth) angle. The UAVs measure signal power at pre-determined ranges and heights in a general direction from the emitter, i.e., the *x*-axis as illustrated in Figure 44. There are two main types of flight patterns: horizontal and vertical. Horizontal flight patterns can be performed by UAVs such as ScanEagle, and a typical profile is illustrated in Figure 45. A vertical flight pattern has to be performed by a rotary-wing platform because of its ability to fly vertically. For the sake of the discussion, we assume a quadrotor as the rotary-wing UAV. The typical profile is illustrated in Figure 46.

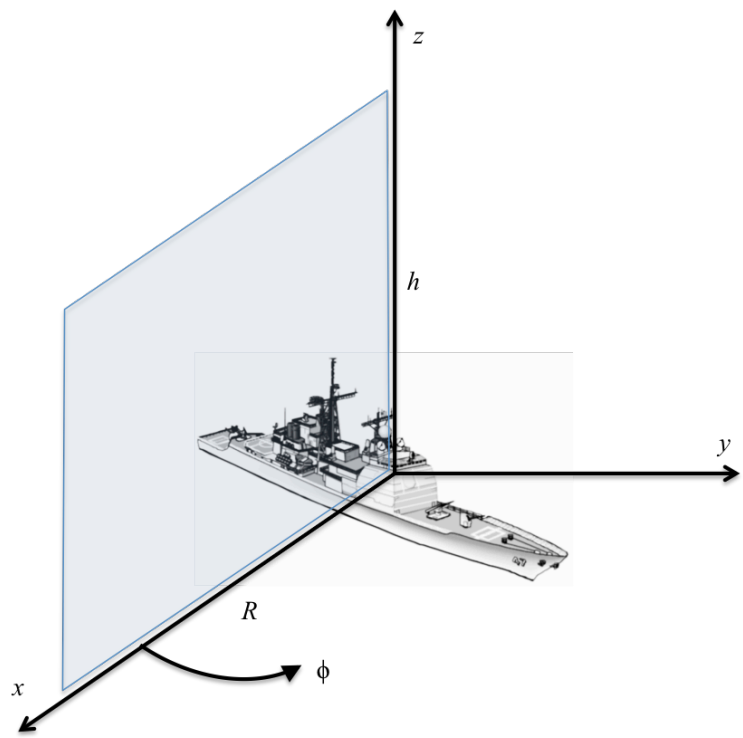

Figure 44. Data Collection in an Azimuth Measurement Plane

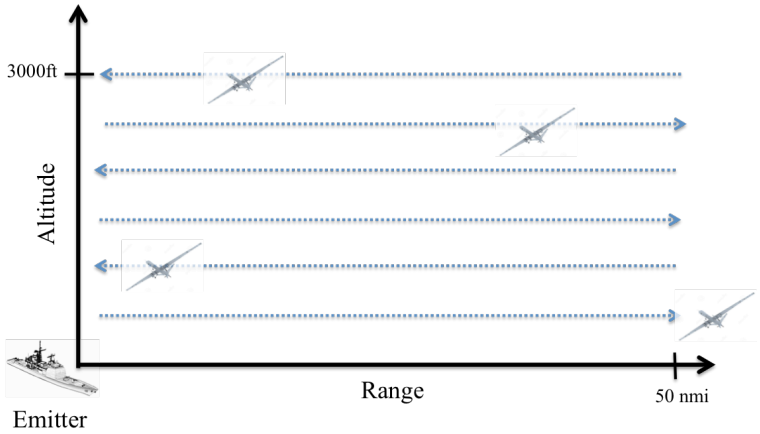

Figure 45. Horizontal Flight Pattern

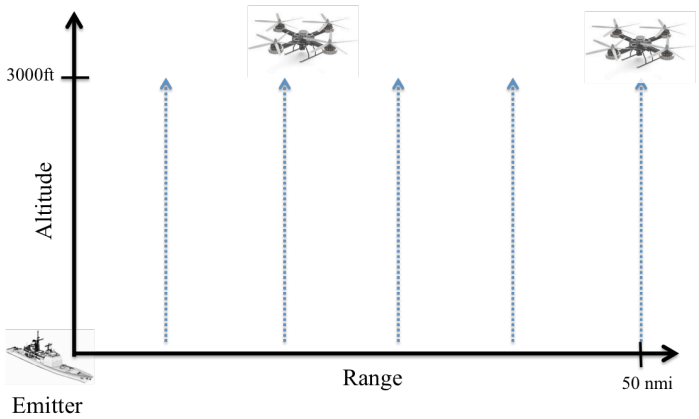

Figure 46. Vertical Flight Pattern

In the horizontal flight pattern, typical UAVs like ScanEagle are not able to "hover" at specified locations to measure signal power; therefore, there are inaccuracies in determining the location of the signal power measurement. To understand the inaccuracies, we need to know the time required to measure a sample t and the cruising speed s of the UAV as this determines the distance d traveled by the UAV while a sample is being taken; i.e.,

$$d = t \times s. \tag{11}$$

The distance d traveled by a ScanEagle cruising at 90 km/h while a sample is being taken for the different types of spectrum analyzers is presented in Table 10. As

seen in the table, the overall inaccuracies due to the distance traveled by the ScanEagle are relatively low since the sample time is relatively fast.

Table 10. Distance Traveled by ScanEagle, One Measurement

Type of Spectrum Analyzers [20]	Sample Time (ms)	Distance Traveled by ScanEagle (m)
Entry Level	100	2.5
Intermediate Level [20]	100	2.5
Professional Level	10	0.25
Professional Level with Pre-amplifier	5	0.125

There is no such issue for the vertical flight pattern as the quadrotor can hover at the specified spot during measurements to avoid such errors.

2. Samples Required

In Chapter IV, we found that the minimum range required to perform both functions is 125 nmi and the minimum number of samples required is 100; however, the minimum range is reduced to 50 nmi and five samples if we only need to detect the presence of atmospheric ducts. In the vertical direction, the minimum height is 3000 ft, and the minimum number of samples required is 30 for both functions (See Table 6); therefore, we would require a minimum of 3000 samples to be able to perform both functions and only 150 samples if we only need to detect the existence of atmospheric ducts.

3. Data Collection Time

The total time required to collect the minimum number of samples depends on the number of UAVs available and the flight pattern. In the horizontal flight pattern, the ScanEagle is assumed to cruise at 90 km/h and takes approximately one hour to fly 50 nmi (i.e., 50 nmi/h); therefore, it takes one ScanEagle an impractical time of

approximately 30 hours to finish scanning 50 nmi and 3000 ft (or one sample per 100 ft) as illustrated in Figure 47.

The data collection times for the horizontal flight pattern to accomplish (1) detecting duct or (2) detecting ducts and determining κ are summarized in Table 11. By increasing the number of ScanEagles, we can reduce the data collection time proportionately.

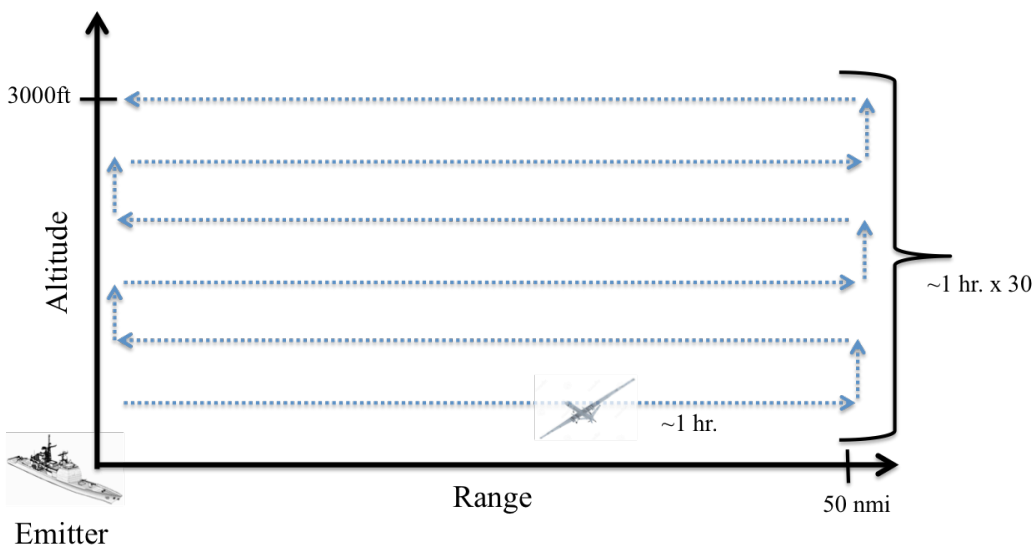

Figure 47. Horizontal Flight Pattern with Estimated Time (Single ScanEagle)

Table 11. Data Collection Times for Horizontal Flight Pattern

Capabilities	Range/ Height	Samples (Range/ Height)	1 UAV	5 UAVs
Detect ducts only	50 nmi/ 3000 ft	5/ 30	~30 hrs.	~6 hrs.
Detect ducts and determine κ value	125 nmi/ 3000 ft	100/ 30	~83 hrs.	~16.6 hrs.

For the vertical flight pattern, the quadrotor is assumed to fly at 30 km/h and hover at specified spots for two seconds to measure the signal power. The flight pattern is illustrated in Figure 48. In the case of five quadrotors, we assume that there are enough

ships or buoys within specified range that the quadrotors can lift off for measurements as seen in Figure 49. The data collection times for both cases are summarized in Table 12. .

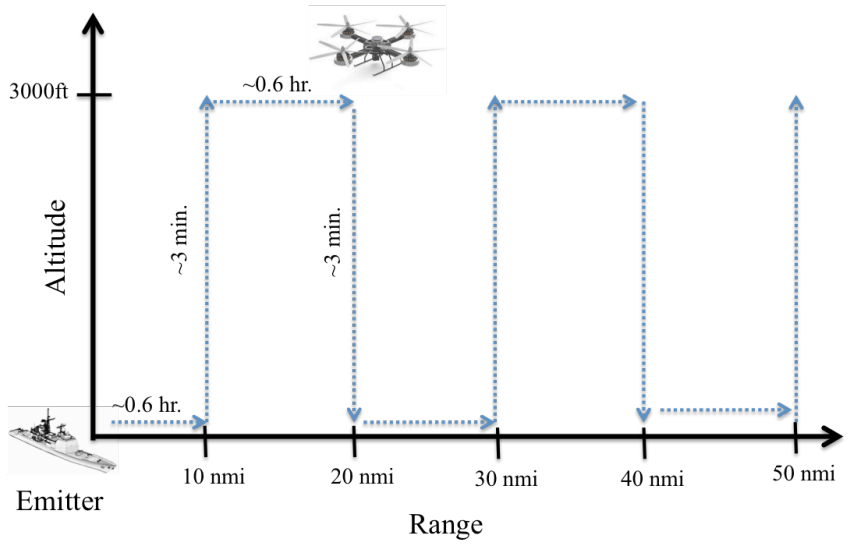

Figure 48. Vertical Flight Pattern with Estimated Time (Single Quadrotor)

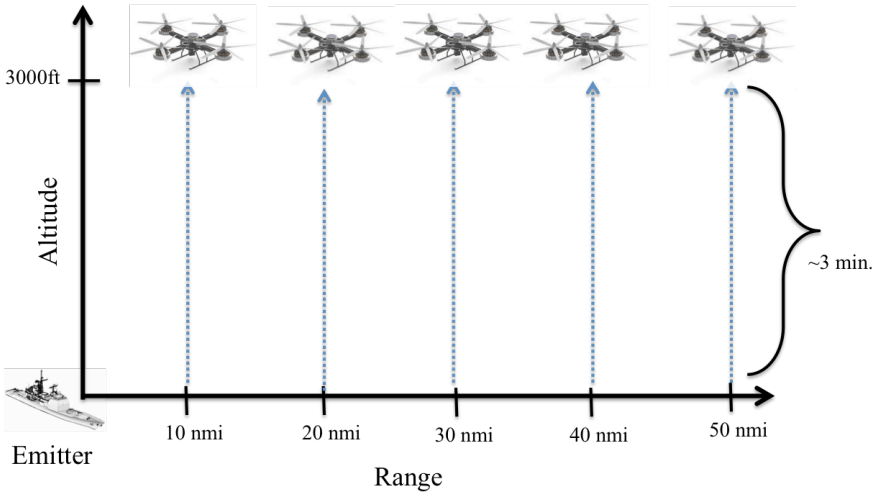

Figure 49. Vertical Flight Pattern with Estimated Time (Multiple Quadrotors)

Table 12. Data Collection Time for Vertical Flight Pattern

Capabilities	Range/ Height	Samples (Range/ Height)	1 Quadrotor	5 Quadrotors
Detect ducts only	50 nmi/ 3000 ft	5/ 30	~3.5 hrs.	~3 min.
Detect ducts and determine κ value	125 nmi/ 3000 ft	100/ 30	~66.6 hrs.	~2.6 hrs.

From Table 11 and Table 12, we observe that the vertical flight pattern is expected to be more efficient and is, therefore, the preferred option for data collection.

F. CHAPTER SUMMARY

In this chapter, the system implementation requirements such as the equipment required to support the propagation loss measurements were discussed. The optimal frequency spectrum was also investigated and recommended. In this chapter, we also examined the flight patterns and the time required to collect the required samples for the developed program to extract the real-time atmospheric data.

VI. CONCLUSIONS AND RECOMMENDATIONS

A. SUMMARY AND CONCLUSIONS

The goal of this research was to investigate the use of UAVs to assess the propagation environment, which allows ship operators to better understand the performance of their radar and communications systems. In this thesis, we presented the basic architecture of the overall envisaged system to collect propagation loss data using UAVs and described some of the system implementation requirements. To ensure accuracy of the measured propagation loss data, our research recommends the UAVs be outfitted with GPS, altimeter, gyroscope, data storage, and local processing capability, which provide the means for the processing computer to correlate transmitter-receiver signal information and take antenna pointing and polarization loss into consideration. Data links between the UAVs and the central processing computer are recommended for quick transfer of data. The different types of flight patterns and their data collection times were studied, and we concluded that the vertical flight pattern using a rotary-wing platform is more efficient and, therefore, recommended. Simulations using AREPS suggested that the optimal operating frequency spectrum is between 2.0 to 4.0 GHz (S Band).

As part of this thesis, we verified the previously developed algorithm and the software's ability to process and extract the propagation environment under multiple scenarios. The software was able to correctly predict the atmospheric refractivity, κ, and the presence of atmospheric ducts in all scenarios using AREPS propagation loss data; however, the verification studies were conducted using large data sets (300 nmi × 10,000 ft, 440 × 384 samples). Since it is not realistically possible to collect such a large data set over vast distances, the minimum data set was examined by gradually reducing the data points as well as height and range from the transmitter. We found that duct sensing requires a minimum range of 50 nmi but requires a minimum of 125 nmi to correctly predict the atmospheric refractivity κ.

B. FUTURE WORK

Going forward it will be worthwhile to conduct field measurements using UAVs or manned aircraft with receivers capable of measuring signal power with known height and range referenced to the transmitter. As the measured propagation loss data is likely to contain multiple sources of errors, this approach will evaluate the algorithm's ability to accurately extract the propagation environment. Additionally, we can also conduct an error tolerance study by adding antenna pointing and location (GPS) errors to the simulation scenarios. We foresee that the algorithm has room for improvement, especially the curve fitting method to extract κ. Improvement in the curve-fitting method may reduce the range and data set required to predict the atmospheric refractivity κ.

LIST OF REFERENCES

[1] A. E. Barrios, "Parabolic equation modeling in horizontally inhomogeneous environments," *IEEE Trans. Antennas Propagat.,* vol. 40, pp. 791–797, 1992. [Online]. doi: 10.1109/8.155744

[2] D. F. Gingras, P. Gerstoft, and N. L. Gerr, "Electromagnetic matched-field processing: Basic concepts and tropospheric simulations," *IEEE Trans. Antennas Propagat.,* vol. 45, pp. 1536–1545, 1997. [Online]. doi: 10.1109/8.633863

[3] P.Gerstoft, D. F. Gingras, L. T. Rogers, and W. S. Hodgkiss, "Estimation of radio refractivity structure using matched-field array processing," *IEEE Trans. Antennas Propag.*, vol. 48, pp. 345–356, 2000. [Online]. doi: 10.1109/8.841895

[4] P. S. Guest and C. Machado, "Using UAS to sense the physical environment and predict the electromagnetic system performance," Monterey, CA, USA, 2014.

[5] "Radar basics: Propagation of electromagnetic waves," radar tutorial by C. Wolff, Jan. 22, 2018. [Online]. Available: http://www.radartutorial.eu/07.waves/wa17.en.html

[6] S. M. Babin, G. S. Young, and J. A. Carlton , "A new model of the oceanic evaporation duct," *J. Appl. Meteorol*., vol. 36, pp. 193–204, 1997. [Online]. doi: https://doi.org/10.1175/1520-0450(1997)036<0193:ANMOTO>2.0.CO;2

[7] A. Karimian, C. Yardim, P. Gerstoft, W. S. Hodgkiss, and A. E. Barrios, "Refractivity estimation from sea clutter: An invited review," *Radio Sci*., vol. 46, RS6013, 2011. [Online]. doi: 10.1029/2011RS004818

[8] A. R. Lowry, C. Rocken, S. V. Sokolovskiy, and K. D. Anderson, "Vertical profiling of atmospheric refractivity from ground-based GPS," *Radio Sci*., vol. 37, no. 3, pp. 1041–1059, 2002. [Online]. doi: 10.1029/2000RS002565

[9] L. T. Rogers, "Likelihood estimation of tropospheric duct parameters from horizontal propagation measurements." *Radio Sci*., vol. 32, no.1, pp. 79–82, 1997. [Online]. doi: 10.1029/96RS02904

[10] C. A. Levis, J. T. Johnson, and F. L. Teixeira, *Radiowave Propagation: Physics and Applications.* Hoboken, NJ, USA: John Wiley & Sons, Inc., 2010, ch. 6, sec. 8, pp. 129–132.

[11] "Propagation near the Earth's surface," class notes for Radiowave Propagation, Dept. of Electrical Engineering, Naval Postgraduate School, Monterey, CA, USA, spring 2017.

[12] "Atmospheric refraction: How electromagnetic waves bend in the atmosphere and why it matters," class notes for Atmospheric Effects on Electromagnetic Systems, Dept. of Meteorology, Naval Postgraduate School, Monterey, CA, USA, spring 2017.

[13] H. W. Ko, J. W. Sari, and J. P. Skura, "Anomalous microwave propagation through atmospheric ducts," *Johns Hopkins APL Tech. Digest*, vol. 4, pp. 12–26, 1983. [Online]. Available: http://www.jhuapl.edu/techdigest/views/pdfs/V04_N1_1983/V4_N1_1983_Ko.pdf

[14] I. M. Brooks, A. K. Goroch, and D.P. Rogers, "Observations of strong surface radar ducts over the Persian Gulf," *J. Appl. Meteorol.*, vol. 38 (9), pp. 1293–1310, 1999. [Online]. Available: http://journals.ametsoc.org/doi/pdf/10.1175/1520-0450%281999%29038%3C1293%3AOOSSRD%3E2.0.CO%3B2

[15] W. L. Patterson, "Advanced refractive effects prediction system (AREPS)," San Diego, CA, USA, 2001. [Online]. Available: http://www.dtic.mil/dtic/tr/fulltext/u2/a434242.pdf

[16] A. E. Barrios, "Considerations in the development of the advanced propagation model (APM) for U.S. Navy applications," in *IEEE Radar Conference*, pp. 77–82, 2003 [Online]. doi: 10.1109/RADAR.2003.1278714

[17] X. Zhao, D. Wang, S. Huang, K. Huang, and J. Chen, "Statistical estimations of atmospheric duct over the South China Sea and the tropical eastern Indian Ocean," in *Chin. Sci. Bull.*, vol. 58, no. 23, pp. 2794–2797, 2013. [Online]. doi: https://doi.org/10.1007/s11434-013-5942-8

[18] S. M. Babin, "Surface duct height distributions for Wallops Island, Virginia, 1985–1994," *J. Appl. Meteorol.*, vol.35, no. 1, pp. 86–93, 1996. [Online]. doi: https://doi.org/10.1175/1520-0450(1996)035<0086:SDHDFW>2.0.CO;2

[19] I. Poole, "Receiver sensitivity," radio-electronics.com, Feb. 5, 2018. [Online]. Available: http://www.radio-electronics.com/info/rf-technology-design/rf-noise-sensitivity/receiver-sensitivity-performance-tutorial.php

[20] Aaronia AG, *Handheld Spectrum Analyzer Spectran V4*, 2015. [Online]. Available: http://www.aaronia.com/Datasheets/Spectrum_Analyzer/Spectrum_Analyzer_Aaronia_Spectran_HF-6000-Series.pdf

INITIAL DISTRIBUTION LIST

1. Defense Technical Information Center
   Ft. Belvoir, Virginia

2. Dudley Knox Library
   Naval Postgraduate School
   Monterey, CA